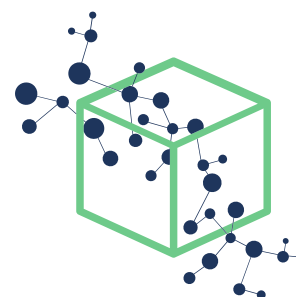


postprint

An atomistic evaluation of the compatibility and plasticization efficacy of phthalates in poly(vinyl chloride)

Li, Panchal, Mafi, and Xi (2018)

DOI: [10.1021/acs.macromol.8b00756](https://doi.org/10.1021/acs.macromol.8b00756)



Xi RESEARCH
<http://xiresearch.org>

This document is the **accepted manuscript (after peer review)** version of an article published in its final form (i.e., the version of record) by American Chemical Society as

Dongyang Li, Kushal Panchal, Roozbeh Mafi, and Li Xi. An atomistic evaluation of the compatibility and plasticization efficacy of phthalates in poly(vinyl chloride). *Macromolecules*, 51: 6997–7012, 2018. doi: [10.1021/acs.macromol.8b00756](https://doi.org/10.1021/acs.macromol.8b00756)

(copyright © 2018, American Chemical Society). The *version of record* is hosted at

<https://dx.doi.org/10.1021/acs.macromol.8b00756>

by the publisher.

The current version is made available for your personal use only in accordance with the publisher's policy. Please refer to the publisher's site for additional terms of use.

BIB_{TEX} Citation Entry

```
@article{LiMacro18,  
  author = {Li, Dongyang and Panchal,  
            Kushal and Mafi, Roozbeh and Xi,  
            Li},  
  title = {{An atomistic evaluation of the  
            compatibility and plasticization  
            efficacy of phthalates in  
            poly(vinyl chloride)}},  
  journal= {Macromolecules},  
  volume = {51},  
  pages = {6997-7012},  
  year = {2018},  
}
```

brought to you by the
Xi RESEARCH GROUP at McMaster University
— www.XiRESEARCH.org —
Principle Investigator:
Li Xi 奚力
Email: li@xiresearch.org

t <https://twitter.com/xiresearchgroup>
in <https://linkedin.com/company/xiresearch/>
RG https://researchgate.net/profile/Li_Xi16
Ⓐ <https://mendeley.com/profiles/li-xi11/>

An atomistic evaluation of the compatibility and plasticization efficacy of phthalates in poly(vinyl chloride)

Dongyang Li^{1,2}, Kushal Panchal², Roozbeh Mafi³, and Li Xi^{*2}

¹School of Chemical Engineering and Technology, Tianjin University, Tianjin 300072, China

²Department of Chemical Engineering, McMaster University, Hamilton, Ontario L8S 4L7, Canada

³Canadian General Tower, Ltd., Cambridge, Ontario N1R 5T6, Canada

August 11, 2018

Abstract

Using full-atom molecular simulation, we report the first systematic investigation of common phthalate plasticizers for PVC. A multi-step model generation and equilibration protocol are proposed for amorphous polymer-plasticizer mixtures, from which statistically robust prediction of materials properties is achieved. Plasticizer performance is evaluated with our molecular models, which considers both their plasticization efficacy and thermodynamic compatibility with

*corresponding author: xili@mcmaster.ca

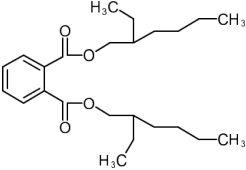
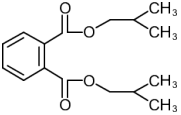
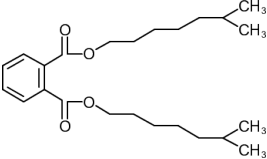
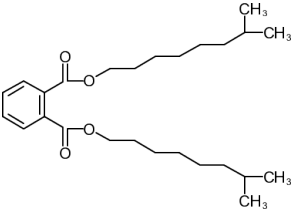
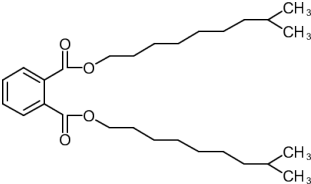
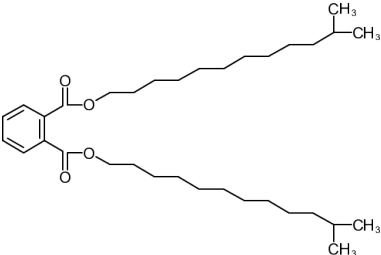
the host polymer. Effects of the alkyl side chain configuration in these phthalates are systematically discussed. The results agree well with all known experimental observations. In addition to the size of the alkyl chains, their branching configuration is another factor affecting the phthalate compatibility with PVC. Relaxation of the alkyl side chains is found to be the limiting step in the diffusion of phthalates in PVC, making it a key design parameter for better migration resistance. With the addition of plasticizers, the dynamics of PVC backbones remain the same in the short-time relaxation process, but an earlier onset of the cooperative motion between molecules allows it to enter the long-time diffusive regime earlier. The main outcomes of this study include (1) a molecular modeling protocol validated with commonly used phthalates, which can be used to predict the performance of alternative plasticizers, and (2) molecular insight that can better inform the molecular design of new plasticizers. As a side outcome, we also report a non-trivial chain-length dependence of the cohesive energy and solubility parameter of long-chain polymers, which is an important consideration in the calculation of these quantities using molecular simulation.

1 Introduction

Thanks to their endless possibilities of molecular design and formulation development, polymer-based engineered plastics are well-poised to address the increasing demand for high-performance and functional materials. Additives are essential ingredients of most plastic formulations and plasticizers account for one-third of the additive market¹. Poly(vinyl chloride) (PVC) is one of the most commonly used thermoplastics and consumes over 80% of all plasticizers on the market². Plasticizers are introduced to adjust the thermo-mechanical properties of materials, such as reducing their glass transition temperature (T_g) and Young's modulus, for improved flexibility and reduced brittleness, as well as to modify their rheological response for better processibility. Adding different amounts of plasticizers, PVC can be manufactured in several grades and applied in different areas, such as building materials, furniture, toys, medical devices, electrical insulation, packaging materials, and food wrappers.

The most widely used type of plasticizers are phthalates (see examples in table 1), which account for 92% of the plasticizer market, and di-(2-ethylhexyl) phthalate (DEHP) takes up more than 50% of the phthalate production³. Popularity of these plasticizers in the industry results from their superb plasticization efficacy, compatibility with PVC, good water resistance, and low cost. However, phthalates are prone to migration loss. Escape of plasticizers from the host polymer contaminates the surrounding environment and causes gradual deterioration of plastics performance over time. Although initially considered benign, phthalates are increasingly associated with potential toxicity and carcinogenic risks in recent years⁴⁻⁷, prompting tightening governmental regulation on their usage, especially in applications such as medical devices, food packaging, and children's toys^{5,7-9}. There is thus an imminent pressure on the plastic industry to find or develop alternative plasticizers. Various compounds are being investigated, including citrates¹⁰, TOTM (tris (2-Ethylhexyl) trimellitate)⁸, Hexamoll DINCH (1,2-cyclohexane dicarboxylic acid diisononyl ester)¹¹, DEHA (di-(2-ethylhexyl) adipate)¹², bis(2-ethylhexyl) azelate⁸, epoxidized vegetable oils⁸, and ionic liquids¹³.

Table 1: Chemical structures of phthalate molecules modeled in this study.

Acronym	Full name	Number of carbon atoms in each alkyl chain	Detailed chemical structure
DEHP	Bis(2-ethylhexyl) phthalate	8	
DIBP	Diisobutyl Phthalate	4	
DIOP	Diisooctyl phthalate	8	
DINP	Diisononyl phthalate	9	
DIDP	Diisodecyl phthalate	10	
DITP	Diisotridecyl phthalate	13	

The vast choice of candidates makes the experimental development an expensive and daunting task. Meanwhile, targeted molecular selection or design is as yet not possible owing to the lack of fundamental knowledge of the plasticization mechanism. Classical theories for plasticization, such as the lubricity theory, gel theory, and free volume theory, are most commonly cited^{14,15}. However, these theories are all phenomenological in nature. They offer convenient arguments for rationalizing certain experimental observations but lack the molecular basis necessary for bottom-up prediction – from the chemicals structure to performance, which is required for guiding molecular design efforts. Despite the long history of the industrial application of plasticizers, systematic investigation of the effects of their molecular structure on plasticization efficacy did not emerge until very recently. Most notably, Erythropel et al.¹⁶ tested the mechanical properties of PVC films blended with succinates and maleates with varying alkyl chain lengths as plasticizers and also compared these compounds with DEHP. It was concluded that for diester plasticizers, the performance peaks with alkyl chains of approximately 4–6 carbons and the central group (i.e., the structure between the esters) has much smaller impact. The molecular mechanism is, however, not easily attainable in experiments.

Molecular modeling and simulation are often resorted to in such situations and its application in polymers has made great strides over the past three decades. The first major challenge, perhaps somehow unexpected to experimentalists, is to generate molecular models representative of realistic amorphous polymer structures. Starting from the seminal work of Theodorou and Suter¹⁷, the classical approach for amorphous cell generation grows or connects repeating units in a stepwise manner until the polymer chains fill the simulation cell^{18–20}. The chain growth algorithm normally follows the physical ansatz of the three-dimensional random walk or rotational isomeric state (RIS) model (which more realistically samples the backbone torsion angle distribution). Geometric or energetic constraints are also imposed to avoid atom overlaps. Indeed, PVC was among the earliest polymers to be modeled at the molecular level: Ludovice and Suter²¹ found that despite its structural similarity

with polypropylene (PP) which was the model system tested by Theodorou and Suter¹⁷, the generation protocol must be adjusted to account for the polarity introduced by the chlorine atoms. This example also showed that the required procedure varies for different polymers and highlighted the importance of validating the model generation protocol for each new system. With the vast improvement of computer hardware, it is now commonly required that the generated chain configuration additionally undergo extended steps of simulated relaxation, which normally includes repeated heating-cooling or expansion-compression cycles, to eliminate local conformational strains and the exact protocol depends on the specific system being modeled. Monte Carlo (MC) approaches that statistically swap the connectivity between chains can also be used for the fast relaxation of chain conformation^{22,23}, but for full-atom models the acceptance ratio decreases sharply as the molecular structure becomes more complex or the backbone stiffness increases. Recent development of the systematic coarse-graining approach provides an alternative solution: the polymer structure can be equilibrated at the coarse-grained level where longer time scales are computationally accessible and the equilibrated structure is then “back-mapped” to the full-atom level^{24,25}.

Building models for polymer-additive mixtures seems to be a direct extension. Previous efforts mostly focused on mixtures with small gas or liquid penetrates where their permeability in polymer matrix is of great interest in applications such as membrane separation^{26–31}. However, plasticizers are very different for their complex molecular structure and much larger size. Unlike small-molecule diluents which can fit easily into the voids between polymer segments in an existing amorphous cell, inserting additives of the size and shape of plasticizers inevitably requires the surrounding polymer segments to retreat to make space. The methodology for generating such structures can follow the same idea as that for pure polymer cells, but the equilibration protocol must be carefully tested for reliable property prediction. To date, there have been only a handful reports on the full-atom model generation of amorphous polymer mixtures with plasticizers or diluent molecules of comparable size and complexity (e.g., drugs)^{32–36}. These studies all relied on the commercial software **Materials Studio**®

and its built-in amorphous cell builder module, whose proprietary algorithm is not known to the public. More importantly, the applications that they targeted at, such as energetic materials (e.g., propellants)^{32,34,36} and pharmaceutical products^{33,35}, require shorter polymer chain lengths in the model: i.e., $O(10)$ repeating units. To our best knowledge, full-atom molecular modeling of plasticized PVC or other engineered plastics, especially comprehensive testing of equilibration protocols for longer chains ($O(100)$ repeating units or more) in the presence of common plasticizers such as phthalates, has not been reported.

Molecular modeling can be a valuable tool for tackling the current plasticizer challenge. Its role in the plasticizer development can be both direct – i.e., helping with the selection or screening of candidate molecules to reduce experimental cost – or indirect – i.e., providing molecular insight into plasticizer actions as theoretical guidelines. Both require the reliable prediction of plasticizer performance. As discussed above, the new criteria for evaluating plasticizers include not only plasticization efficacy but also their migration resistance. The former is measured by the extent of property improvement at a certain plasticizer dosage. Molecular simulation prediction of the thermo-mechanical properties, such as T_g and the stress-strain relationship, has been well-established for pure polymers (linear and crosslinked), polymer blends, and nanocomposites^{37–46}. Studies of plasticized polymers are much less³⁵ and for engineered plastics such as PVC-phthalate mixtures it is still a void to fill (as mentioned above). Migration rate is much harder to predict directly because the time scale of molecular diffusion for molecules as large as phthalates are beyond what is accessible in full-atom molecular simulation^{28,47–49}. Nevertheless, migration tendency of a plasticizer can be at least partially estimated based on its thermodynamic affinity with the host polymer. The Hildebrand solubility parameter δ , available from molecular simulation by calculating the cohesive energy density (CED)⁵⁰, is often used to estimate the thermodynamic compatibility between components. It was widely used for estimating plasticizer compatibility with the host polymer^{32,34,36,51}. However, again, application in engineered plastics such as PVC-phthalate mixtures has not been reported.

This study is the first systematic investigation of the performance of common industrial plasticizers in PVC. It builds on decades of progress made in computational polymer science and is the first step in our ongoing effort aiming at incorporating molecular simulation into the toolbox for the design and discovery of high-performance plasticizers. There are two main objectives. The first is to test and establish the model generation and equilibration protocol for plasticized polymers. Although the molecular modeling of amorphous polymer cells has been developed for decades, its application in polymers blended with diluent molecules as large as plasticizers is rarely reported. In this study, a multi-step equilibration protocol will be tested and validated using common phthalate plasticizers for which more data are available for comparison. The established protocol will then be used in our future study of newer alternative plasticizers. The second objective is to systematically evaluate and compare common phthalates and study the effects of molecular design parameters, in particular, alkyl side chain configurations, on their performance. In the context of the current plasticizer challenge, the new paradigm for evaluating plasticizer performance must simultaneously consider its plasticization efficacy, thermodynamic compatibility with the host polymer, and migration resistance. Understanding the effects of molecular structures on these performance metrics will offer new guidelines for the molecular design of next-generation plasticizers. Phthalates listed in table 1 are chosen for this purpose because they share strong chemical similarity and only differ in their alkyl side chains. Among them, DIBP, DIOP, DINP, DIDP, and DITP are nearly identical except their different alkyl chain lengths, whereas DIOP and DEHP both have eight-carbon alkyl chains but they differ in the branching configuration. Direct comparison between these compounds will offer the first insight into the effects of the alkyl side chain on the performance of phthalate plasticizers. (Recall that according to the experiments of Erythropel et al.¹⁶, at least for succinates and maleates, the side chain configuration is the most influential molecular parameter for plasticization efficacy.) Through our study, we also realized two important considerations in the calculation of cohesive energy (and thus solubility parameter) in molecular simulation: the ambiguity

of the choice of reference state⁵² and the non-trivial chain-length dependence. The second one is to our best knowledge reported for the first time. These quantities are widely used in the literature for evaluating thermodynamic properties of polymers and implications of these two considerations will be discussed.

2 Simulation details and equilibration protocol

2.1 Molecular and simulation details

Full-atom molecular models are used and the potential energy is calculated with the polymer consistent force field (PCFF)^{53,54}. PVC molecules are end-capped with H and CH₃ and has the chemical formula of H-(CH₂CH(Cl))_n-CH₃ (n being the degree of polymerization). All PVC chains in this study are atactic. (Recent study of another polymer similar to PVC, poly(vinyl alcohol) (PVA), showed that tacticity affects solubility parameter but all other properties studied, including the density and T_g , are insensitive to the PVA tacticity⁵⁵.) Structures for the phthalate molecules are provided in table 1. Molecular dynamics (MD) simulation is implemented with the Large-scale Atomic/Molecular Massively Parallel Simulator (LAMMPS)⁵⁶, an open-source MD engine. The cutoff distance for pairwise – van der Waals (vdW) and electrostatic – interactions is set at 15 Å. Long-range vdW interaction is approximated by the tail correction^{57,58} and long-range electrostatic interaction is computed with the standard Ewald summation method^{58–60}. Time integration is performed with the standard velocity-Verlet algorithm with a time step of 1 fs and energy minimization is performed with conjugate gradient algorithms^{58,59}. The thermo- and baro-stats, when applied, are realized with Nosé-Hoover chains⁶¹.

2.2 Amorphous cell: preparation and equilibration protocol

Both the PVC chains and plasticizer molecules are constructed in **Xenoview**, an open-source software for molecular modeling and graphics⁶². PVC chains are packed into a cubic

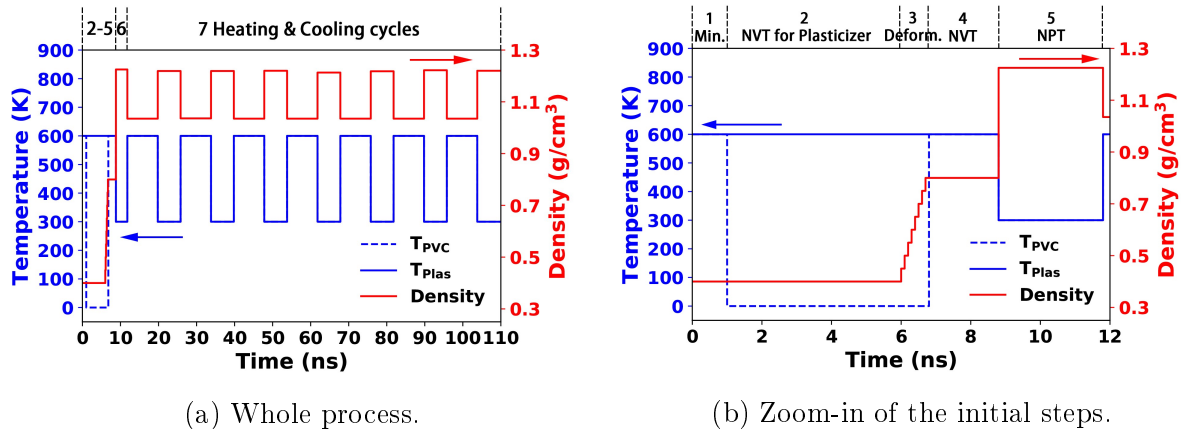
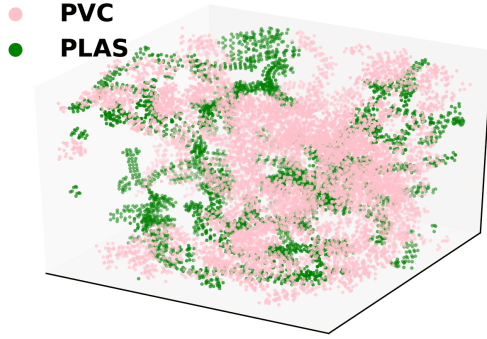


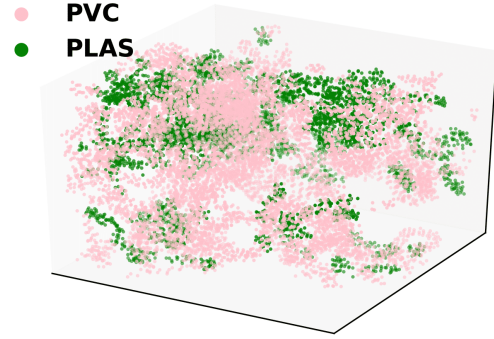
Figure 1: Temperature and density profiles during the amorphous cell generation process for the PVC/DITP mixture.

simulation cell also by **Xenoview**, which generates polymer chains in a periodic box by sampling backbone torsion angles according to their RIS distribution. This is similar in spirit to the original Theodorou and Suter¹⁷ method except that the latter further introduced a correction to the sampling probability based on the non-bonded interactions between the new repeating units and existing ones (instead of a simple geometric constraint to avoid atom overlaps in **XenoView**⁶³). It was shown that this probability correction does result in statically different chain configurations^{17,21} compared with a pure RIS approach. However, the comparison was between chain configurations after energy minimization only. In our case, the amorphous cell configuration from **XenoView** further undergoes an extensive multi-step equilibration protocol (see below), during which torsion angles will have adequate time to relax to the new distribution under the influence of full non-bonded interactions, which, therefore, will erase any difference in chain conformation caused by the lack of this specific treatment in the initial chain growth step. The initial configuration is built (in **XenoView**) at a low density ($<0.5 \text{ g/cm}^3$). This loose initial packing leaves sufficient room for plasticizers, which are inserted into the voids between chain segments by Packmol⁶⁴.

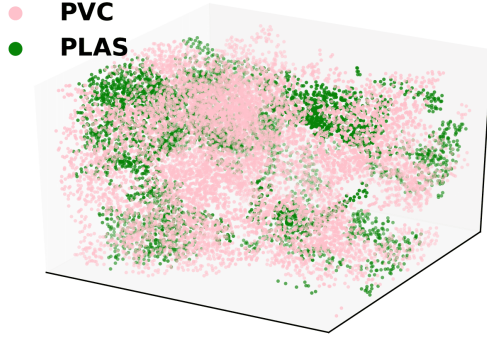
The structure needs to be further equilibrated before production runs. Through our trial and error, the following multi-step amorphous cell building procedure is found to render most robust prediction of all properties relevant to this study.



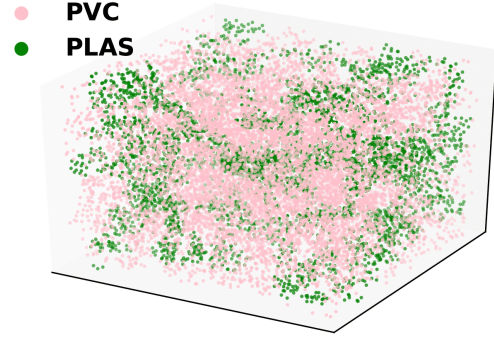
(a) After step 2 ($L_{box}=79.00\text{\AA}$)



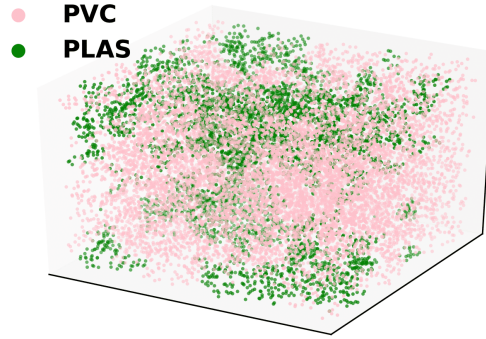
(b) After step 4 ($L_{box}=79.00\text{\AA}$)



(c) After step 5 ($L_{box}=62.72\text{\AA}$)



(d) After step 6 ($L_{box}=54.52\text{\AA}$)



(e) After step 7 ($L_{box}=54.48\text{\AA}$)

Figure 2: Spatial distribution of the two components in the PVC/DITP mixture at different stages of the equilibration process: pink(light) – PVC atoms; green(dark) – plasticizer atoms. The images have different densities and are not plotted to scale.

- Step 1** Molecular construction, force-field assignment, RIS chain generation, and plasticizer packing (with `Xenoview` and `Packmol`). Density of the initial cell (polymer+plasticizer) is within 0.35 g/cm^3 to 0.45 g/cm^3 .
- Step 2** Energy minimization to remove atom overlaps and energy singularities.
- Step 3** Keep the density constant and the polymer configuration frozen and run extended ($\approx 5 \text{ ns}$) NVT simulation at 600 K to quickly relax and redistribute the plasticizer molecules.
- Step 4** Shorter ($\approx 2 \text{ ns}$) NVT run for the whole system at 600 K to simultaneously relax both components.
- Step 5** Gradually ramp up the density to 0.8 g/cm^3 over a period of 1 ns with MD at 600 K .
- Step 6** Short (2 ns to 3 ns) NPT run at 1 atm and 300 K for the density to converge.
- Step 7** Repeated (5-7) heating-cooling cycles – each with an 8 ns run at 600 K followed by a 5 ns run at 300 K , both NPT at 1 atm .

Time series of the temperature and density variations during this multi-step protocol is shown in fig. 1 for the PVC/DITP mixture as an example and instantaneous images showing the spatial distribution of the two components are provided in fig. 2. It is clear that although the initial configuration (after **Step 2**) appears well-mixed, the final equilibrated structure is much more homogeneous.

The density of the final equilibrated cell, for this particular mixture, is 1.22 g/cm^3 . For every mixture composition reported in this study, three random configurations are generated at **Step 1**, purposefully at three different initial densities – 0.35 g/cm^3 , 0.40 g/cm^3 and 0.45 g/cm^3 , to test any potential memory effect of the initial configuration. As shown later in table 4, in all cases, structures generated at different initial densities converge to nearly the same final density after the equilibration steps. Predicted values of other quantities of interest, such as the solubility parameter, heat of mixing, and T_g are all found to be independent of the initial configuration, which will be shown in the next section. In this paper, uncertainties in the results are all reported using the standard error of measurements

from these three independent configurations.

The repeated heating-cooling cycles at the end of the protocol are a common approach in the equilibration of polymer amorphous cells. Meanwhile, through our testing, **Step 3** turns out to be uniquely important for modeling amorphous polymer mixtures with plasticizers and, by extension, any diluent molecule of comparable size. Initial conformations of the plasticizer molecules constructed from `Xenoview` do not necessarily reflect the correct statistical distribution of plasticizers in the polymer matrix and their initial spatial distribution in the polymer matrix, as determined by `Pacmol`, is also not natural. It is important to relax the plasticizer structures and allow them to sufficiently sample the polymer matrix, before the density is ramped up and their conformations become locked in. In **Step 3**, the polymer configuration is kept frozen (thus the temperature of PVC is 0 K in fig. 1) because otherwise the chain segments can be pulled towards certain plasticizers, which causes the closing of certain voids in the matrix and prohibits the movement and relaxation of those plasticizers molecules. In certain cases, the whole polymer matrix collapses around some of the plasticizer molecules, which leaves many others out of the mixture and causes effective phase separation in the cell. With the polymer scaffold frozen at a relatively low density, plasticizers are able to flip their conformations and diffuse across the cell rather quickly at the high temperature (600 K) imposed thereon. Indeed, over the 5 ns period used, the mean square displacement (MSD) of even the largest plasticizer molecule tested, i.e., DITP, has exceeded 5000 \AA^2 – approximately the domain dimension squared. Each plasticizer molecule is thus given the opportunity to sample most, if not all, of the cell.

This step is particularly important for the reliable prediction of T_g . In this study, T_g of an amorphous cell is determined by a controlled cooling simulation starting from a temperature (500~600 K) that is much higher than its T_g (see fig. 3; note: data points at higher T are not shown in the figure). NPT simulation needs to be run at the highest temperature for at least 5 ns to fully equilibrate the structure at the high-temperature end. A stepwise cooling process follows: in each step, NPT is run for 1 ns and specific volume is averaged over the last 0.5 ns,

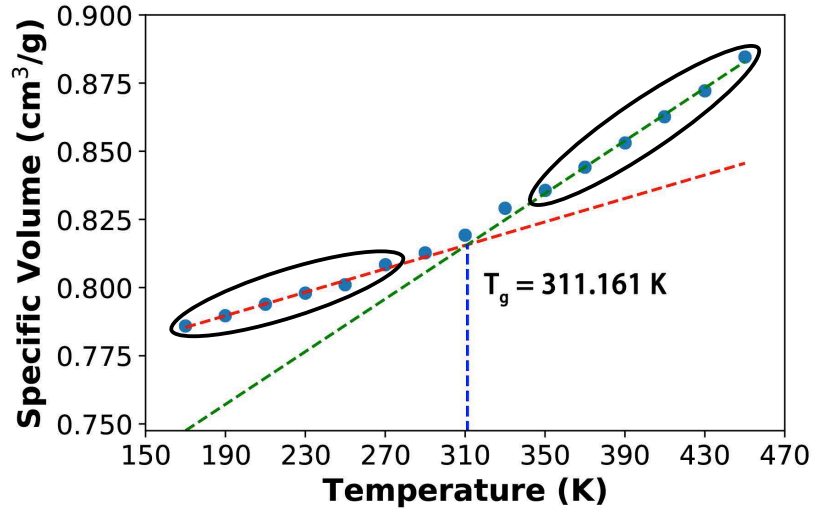


Figure 3: Determining T_g from the temperature dependence of the specific volume for the PVC/DITP mixture.

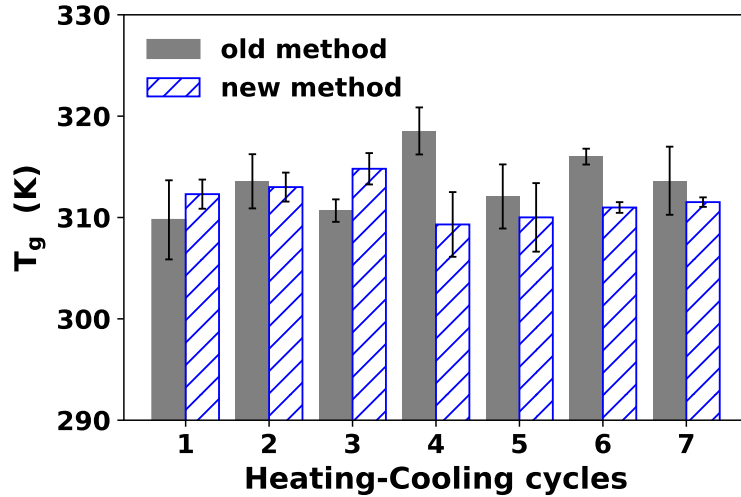


Figure 4: Comparison of the T_g values of the PVC/DITP mixture calculated from the simulation cells equilibrated with the old method (i.e., without **Step 3** and **Step 5**) and with the current (new) method, after different numbers of heating-cooling cycles.

after which the temperature is dropped by 20 K to start the next step. This is an effective cooling rate of 20 K/ns. The temperature dependence of specific volume shows a sharp turn of slope around the glass transition. Both slopes (before and after the transition) are determined using linear regression of at least 5 to 6 points in each case (circled in fig. 3) and T_g is determined by the intersection of these regression lines. Figure 4 shows the comparison of our current equilibration protocol with an older method we tested which did not include **Step 3** and **Step 5**. It is clear that without properly relaxing the plasticizer conformations before the heating/cooling cycles, the T_g prediction fluctuates strongly between cycles and the error bar (standard error of cells from different initial configurations at **Step 1**) remains large after the cycles. Using our current protocol, the prediction converges after cycle 6 and the error bar is reduced to ≤ 2 K. The initial relaxation of plasticizers is also found to be important for the prediction of the heat of mixing (not shown here).

3 Results and discussion

Properties of PVC plasticized with different phthalates as well as those of pure PVC are evaluated and compared in this section. Unless otherwise noted, properties are all reported at 300 K. We start with an extensive validation of our equilibrated amorphous cells by comparison with existing experimental and simulation data in the literature. The choice of the model make-up – the number of molecules and polymer chain length – is also discussed in detail. This is followed by the performance evaluation of different phthalates, including both their compatibility with PVC and plasticization efficacy, and discussion of the alkyl side chain effects. We will conclude with the molecular mobility of different components, which is important for understanding the molecular mechanism of plasticization as well as predicting the migration rate of these additives.

Table 2: Predicted solubility parameter (δ), glass transition temperature (T_g) and density (ρ) of pure PVC cells with different combinations of the chain length (N_{DP}) and number of chains in the cell (N_{chains}), compared with reference values.

		N_{DP}	N_{chains}	δ (J/cm ³) ^{$\frac{1}{2}$}	T_g (K)	ρ (g/cm ³)
Our Results		100	15	17.3 ± 0.026	354 ± 3.53	1.35 ± 0.021
		300	5	17.1 ± 0.172	359 ± 2.67	1.35 ± 0.011
		500	3	16.6 ± 0.108	361 ± 1.58	1.35 ± 0.012
		1500	1	14.6 ± 0.016	354 ± 3.16	1.35 ± 0.014
Reference	Expt.	-	-	19.35^{65}	355.5^{66}	$1.35 \sim 1.45^{67}$
	MD ⁴¹	100	2	17.61 ± 0.45	350	1.39

^aDensity and solubility parameters are reported for 25 °C for experiments and 300 K for MD.

3.1 Model construction and validation

3.1.1 Properties of pure PVC cells

To validate our molecular model and equilibration protocol, we start with the pure PVC case where data are most available in the literature. Previous studies on the molecular simulation of PVC all focused on relatively short chains ($\lesssim 150$ repeating units)^{41,68,69}. Note that the entanglement molecular weight for PVC, according to experiments^{66,70}, is $M_e \approx 5400$ g/mol, which corresponds to $N_e \approx 87$ repeating units. Simulation of PVC chains much longer than this threshold has not been reported. (Ludovice and Suter²¹ studied a longer chain with 200 repeating units but only its conformation from the chain growth algorithm for amorphous cell generation, followed by energy minimization without MD.) As stated earlier, we are interested in the properties at the long-chain limit, which is closer to real PVC plastics. Meanwhile, the computational cost and difficulty of generating RIS chains increase rapidly with the chain length. In table 2 four different amorphous cell compositions are tested, all with the same total number of repeating units (1500) but different degrees of polymerization: 100, 300, 500 and 1500. In all cases, the level of uncertainty in our prediction is at about 1% or less of the mean value, indicating that our equilibration protocol has fully

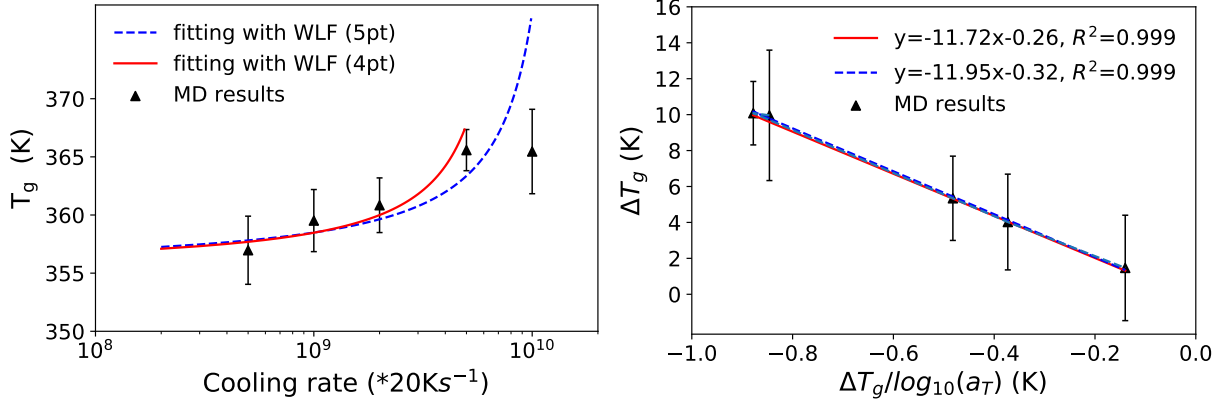


Figure 5: Left: effects of cooling rate on the T_g of pure PVC from MD simulation (5 chains with $N_{\text{DP}} = 300$); right: same data plotted in the coordinates of the linearized form of the WLF equation (eq. (4)). Blue (dashed) and red (solid) lines are the linear regression results based on eq. (4) using all five points and four points (excluding the highest-cooling-rate case), respectively.

relaxed the structure and eliminated any initial configuration dependence. The predicted density is nearly invariant with increasing chain length and in excellent agreement with experimental reports.

Our T_g results from MD are also very close to the experimental value, which would be desirable for most other properties but for T_g it is at least unexpected and requires closer inspection. This is because T_g is a dynamic property that depends not only on the material itself, but also on the cooling rate of its measurement. Cooling rates in MD (e.g., 20 K/ns used in this study) are usually more than 10 orders of magnitude higher than that of experiments (hereinafter, we will use 20 K/min as a representative experimental cooling rate for estimation purpose). It is thus common to see T_g in MD exceeding the experimental value by $O(100)\text{K}^{71,72}$. In comparison, our result certainly appears to be an outlier. We first note that at the same chain length $N_{\text{DP}} = 100$, our T_g result is in excellent agreement with that of Luo and Jiang⁴¹ (the difference is no larger than statistical uncertainty), which used **Materials Studio**[®] and the COMPASS force field⁵⁷. We may thus rule out procedural errors in our calculation. In addition, Luo and Jiang⁴¹ used a much smaller simulation box with only 2 chains – i.e., a total of 200 repeating units versus our 1500 – system size dependence is

also unlikely the reason. Note further that because of our extensive equilibration steps, we are able to obtain two well-defined linear regimes in every specific volume vs. temperature curve (e.g., fig. 3) with a clear-cut transition. Therefore, ambiguity in T_g determination by linear regression (a common problem in this approach) is also avoided. Lastly, although the experimental samples typically have higher molecular weight, the chain-length dependence of T_g is already weak for the range used in this study. In table 2, T_g increases slightly from $N_{\text{DP}} = 100$ to 300, but between $N_{\text{DP}} = 300$ and 500, it has nearly converged. (There is a small unexpected dip in the longest $N_{\text{DP}} = 1500$ case, for which we have no ready explanation. Note, however, that this case differs from the rest as the only single-chain cell: the chain interacts only with its own periodic images which are constrained to the same conformation and always move in sync with the original image.) If we fit the $N_{\text{DP}} = 100, 300$ and 500 points to the Flory-Fox equation⁷³

$$T_g = T_g^\infty - \frac{K}{N_{\text{DP}}} \quad (1)$$

(K is a species-specific constant), the predicted value at infinite chain length $T_g^\infty = 362.73K$, which is still close to the experimental value.

The only reasonable explanation left is that for PVC, or at least its molecular model based on PCFF (and also COMPASS as shown in the case of Luo and Jiang⁴¹), the cooling-rate dependence of T_g is unusually (compared with other polymers) weak. This is not a far-fetched hypothesis. The apparent T_g at a given cooling rate is determined by the relaxation time of the material: glass transition is observed when the material falls out of equilibrium within the time scale of the measurement. Temperature dependence of the relaxation time as a material approaches glass transition is described by its fragility⁷⁴. For fragile glass formers, whose temperature dependence deviates significantly from the Arrhenius behavior, T_g may not vary much over a certain range of temperature. Indeed, PVC happens to be the most fragile polymer that has been experimentally tested^{74,75}.

For a pure PVC cell containing 5 chains with $N_{\text{DP}} = 300$ each, we have tested the T_g for cooling rates varying over more than one decade – 10 K/ns to 200 K/ns (i.e., $(5 \times 10^8 - 1 \times 10^{10}) \times 20$ K/s using the coordinate of fig. 5). Temperature-dependence of the relaxation time is often modeled with the Williams-Landel-Ferry (WLF) equation^{71,72}

$$\Delta T_g \equiv T_g - T_{g,\text{ref}} = -\frac{C_2 \log_{10} a_T}{C_1 + \log_{10} a_T} \quad (2)$$

where

$$a_T \equiv \frac{\tau}{\tau_{\text{ref}}} = \frac{\dot{q}_{\text{ref}}}{\dot{q}} \quad (3)$$

is the time-temperature superposition shift factor, τ is the relaxation time, \dot{q} is the cooling rate, C_1 and C_2 are species-specific constants, and “ref” denotes values at a reference temperature. Equation (2) is rearranged to a linear form

$$\Delta T_g = -C_1 \frac{\Delta T_g}{\log_{10} a_T} - C_2 \quad (4)$$

with which linear regression is performed using the MD data in fig. 5. The reference point is defined as the experimental limit of $T_{g,\text{ref}} = 355.5$ K and $\dot{q}_{\text{ref}} = 20$ K/min. Regression using all five cooling rates tested renders a close fit ($R^2 = 0.999$) with $C_1 = 11.95$ and $C_2 = 0.32$ K. Note that in eq. (2), C_1 determines the singularity point – ΔT_g diverges at $\log_{10} a_T = -C_1$, whereas C_2 determines the rate of divergence. Compared with the so-called “universal” WLF constants of $C_1 = 17.44$ and $C_2 = 51.6$ K often used in experiments as a first estimate for common linear amorphous polymers⁷³, our $C_2 = 0.32$ K for PVC is two orders of magnitude lower, which is consistent with the hypothesis that for PVC the cooling rate dependence is much lower because of its high fragility. Note that our data at the highest cooling rate 200 K/ns is statistically less reliable and clearly does not follow the same trend line as the rest, because the short duration at each temperature level is not sufficient for

averaging. We have repeated the regression excluding this point and the resulting four-point fitting is equally good in the ΔT_g vs. $\Delta T_g / \log_{10} a_T$ coordinates. In the original ΔT_g vs. \dot{q} coordinates, the two regression lines agree well except at the high-cooling-rate limit. (This discrepancy does not show up in the ΔT_g vs. $\Delta T_g / \log_{10} a_T$ plot because errors in ΔT_g affect both coordinates). Outcomes from both regression scenarios show that the simulated T_g at different cooling rates extrapolates well to the experimental T_g with a very weak cooling-rate dependence.

Unlike density and T_g , the solubility parameter δ shows a strong dependence on the chain length with no sign of convergence. More strangely, δ of the shortest chain length in the table (i.e., 100 repeating units) is closest to both the experiment and previous MD report. Some discrepancy with experiments is expected, such as that between the values of the $N_{DP} = 300$ cell ($\delta = 17.1 \text{ (J/cm}^2\text{)}^{1/2}$) and experiment ($\delta = 19.35 \text{ (J/cm}^2\text{)}^{1/2}$). Previous MD predictions of polymer solubility parameters all underestimated the experimental value with similar discrepancies^{17,76}, including both previous studies of PVC^{21,41}. Although MD prediction accuracy is intrinsically limited by the quality of the force-field and the representativeness of the amorphous model, much of this discrepancy comes from the experimental side. Exact measurement of the solubility parameter requires the heat of vaporization, since its definition relies on obtaining the energy of an isolated molecule (see eq. (5) below) – i.e., in a vapor phase. Clearly, for polymers, vaporization is not possible and thus δ is only measured indirectly. A typical procedure would test the polymer solubility in a spectrum of reference solvents with gradually increasing δ of themselves. The solubility parameter of the polymer is reported as the midpoint of the δ range of solvents in which it is soluble⁶⁵. Not only does the measured δ come with large uncertainty, there is also a systematic error owing to the different conformation of polymers in solvents. This error was discussed in detail and a correction was proposed in the recent study by Wu et al.⁷⁶. Nevertheless, what does appear to be incomprehensible in our δ is its increasing deviation, from both the experiment and another MD study, with polymer chain length, which certainly warrants further investigation.

After all, because polymer chains in molecular simulation are generally shorter than those in experiments, one would expect the MD prediction of most quantities to converge closer to the experiments at the long-chain limit.

3.1.2 Chain-length dependence of the polymer solubility parameter

The Hildebrand solubility parameter δ is defined as the square root of the CED

$$\delta^2 \equiv \frac{E_{\text{coh}}}{V} = \rho E_{\text{coh}} \equiv \text{CED} \quad (5)$$

and CED is the cohesive energy per unit volume. Here $V = 1/\rho$ is the specific volume (unless otherwise noted, in this paper extensive properties represented by capital letters are all reported on a per unit mass basis; to represent un-normalized or total property for a given amount of materials, superscript “t” is used: e.g, V^t) and the specific cohesive energy

$$E_{\text{coh}} \equiv E_{\text{sep}} - E_{\text{bulk}} = \frac{\langle E_{\text{ind}}^t \rangle}{m_{\text{ind}}} - E_{\text{bulk}} \quad (6)$$

is the energy it takes to overcome the intermolecular interactions in the condensed phase and pull these molecules apart to infinite separation. The specific potential energy in the condensed phase E_{bulk} is taken directly from the equilibrated cell and the specific potential energy of molecules at infinite separation E_{sep} is the average potential energy of individual molecules when placed in a vacuum $\langle E_{\text{ind}}^t \rangle$ divided by the mass of the molecule m_{ind} . For each system, five molecules are randomly picked and each is moved to a vacuum cell (large empty domain where it does not interact with any other molecules, including its own periodic images) while being frozen in its condensed phase conformation (reason discussed below). Potential energy of the isolated single molecule cell is taken as E_{ind}^t and the average over these five randomly-chosen conformations is found to render sufficient statistics for the average.

In table 2, both the chain length and number of chains are changing. To separate the effects of these two parameters, the solubility parameter of PVC is calculated for a wide

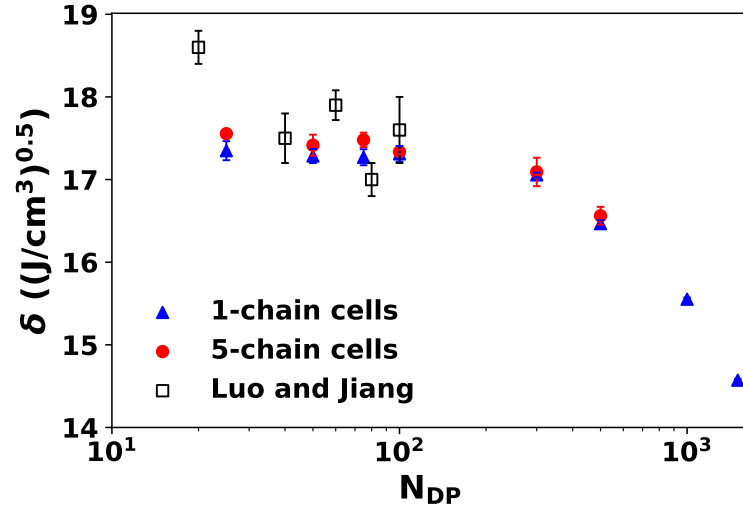


Figure 6: Chain length dependence of the pure PVC solubility parameter using single-chain and five-chain simulation cells, compared with the reference case of Luo and Jiang⁴¹.

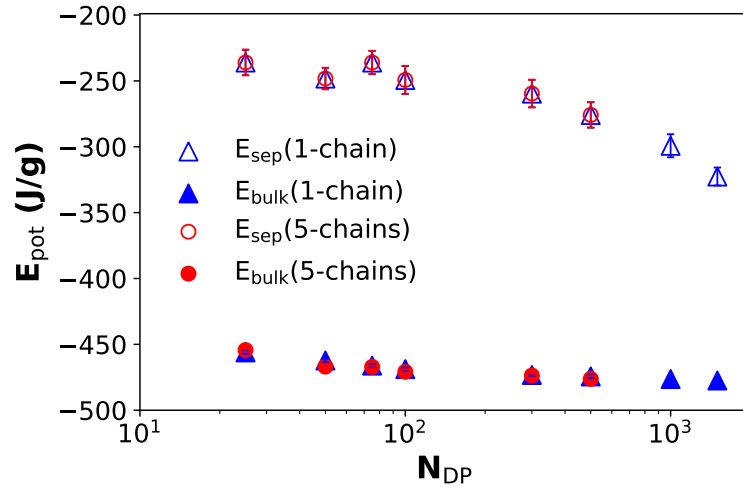


Figure 7: Breakdown of the components of the cohesive energy and their chain length dependence in single-chain and five-chain cells.

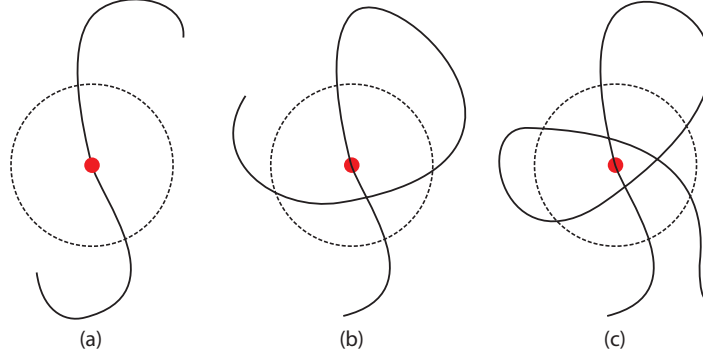


Figure 8: Schematics of the chain-length dependence of the potential energy of an isolated chain.

range of chain length in a single-chain cell (one chain in each periodic box, which still interacts with its own periodic images) and a five-chain cell. The result is plotted in fig. 6 in comparison with δ calculated by Luo and Jiang⁴¹. Luo and Jiang⁴¹ observed some chain length dependence at the short-chain limit, which is expected owing to the chain end effect, but for the degree of polymerization beyond 30 to 40, δ converges. We observe the same plateau in the range between 30 and 100, but as the degree of polymerization exceeds 100, which has not been explored before, δ quickly declines. Results from the single-chain and five-chain cells are well in agreement with each other for all cases tested (five-chain cell for the degree of polymerization $N_{\text{DP}} \geq 1000$ is computationally prohibitive), which rules out any system size effect. Recall that the calculation of δ requires the cohesive energy (eq. (5)), which is the difference between E_{sep} and E_{bulk} . These two energy components are plotted separately in fig. 7. The specific potential energy is nearly the same for longer chains ($N_{\text{DP}} \geq 100$) between the amorphous cells tested – with different chain lengths and different system sizes. Therefore, the chain-length dependence solely comes from the E_{sep} component.

This analysis suggests that the observed chain-length dependence of the solubility parameter or cohesive energy is not an artifact of the limited system size or chain length. Instead, it roots in the definitions of these quantities. Consider $-E_{\text{coh}} = E_{\text{bulk}} - E_{\text{sep}}$ as the system

potential energy using the infinitely-separated chains as the reference state. Here, the calculated system property (E_{bulk}) has well converged, but the reference state energy E_{sep} changes with chain length. When a chain is isolated in a vacuum, its potential energy comes from the bonded and non-bonded interactions. The former does not change with chain length, but for the latter, the dependence is nontrivial. Our proposed explanation is illustrated in fig. 8. For each unit in the chain, the non-bonded interaction only reaches a sphere of the cutoff diameter. For most units, the number of neighboring units along the chain sequence it can reach within the sphere is fixed, except for units near the chain ends where there are fewer peers accessible. This chain end effect is more pronounced in short chains (panel (a)), which explains the chain-length dependence at the small N_{DP} limit (fig. 6 and ⁴¹). As the chain length increases, the chain end effect diminishes with the two ends taking a smaller proportion of the chain, which explains the convergence of E_{coh} and δ at intermediate N_{DP} . Further increasing the chain length can trigger another effect: other units sufficiently far away down the chain sequence can fold back (when the contour distance between the units \gg the persistence length of the polymer) and reenter the interaction sphere of the reference unit (panel (b)). On average, this type of close contacts between units from different parts of the same chain increases with increasing chain length (panel (c)), which brings down the calculated energy E_{sep} and thus E_{coh} and δ . Further validation of the proposed mechanism and theoretical analysis of this chain length dependence is a focus of our ongoing research.

3.1.3 Discussion: chain-conformation considerations for cohesive energy

Cohesive energy and solubility parameter are widely calculated in molecular simulation, including simulation of polymers. In the case of long-chain polymers, our experience in this study reveals that the chain conformation used for calculating E_{sep} has nontrivial effects on the cohesive energy, which should not be overlooked. These effects, again, are not simulation artifacts but an intrinsic part in the definition of cohesive energy. There are two specific considerations. The first is in the model construction of the reference state – isolated chain

in a vacuum – which gives E_{sep} . In this study, the individual polymer chain keeps its conformation in the condensed phase (amorphous cell) when it is moved to a vacuum domain where all intermolecular interactions, including those with its own periodic images, are stripped away. The same approach was taken by Theodorou and Suter¹⁷ and Ludovice and Suter²¹, which took cohesive energy at face value as “the increase of internal energy U per mole of substance if all intermolecular forces are eliminated”⁷³. Alternatively, one may as well build one single chain surrounded by a vacuum and relax its conformation with MD in the absence of intermolecular interactions. Under such a condition, the chain will collapse into a tight coil owing to the interactions between its repeating units – the vacuum surrounding is effectively a poor solvent, resulting in much lower values of cohesive energy and solubility parameter for the same E_{bulk} . Choi and his coworker first recognized this ambiguity and thoroughly studied this issue over 15 years ago^{52,77}. Most other studies in the literature, however, did not specify how the reference state of isolated chain in a vacuum was constructed. We choose to use the first approach because it is conceptually more straightforward: it defines E_{coh} has the intermolecular interactions without the complexity of conformation change. It should be emphasized that the choice does not impact any of our conclusions.

The second consideration is the nontrivial dependence on the chain length at the long-chain limit, which again affects the reference state energy E_{sep} . This effect, as discussed above, is likely a result of chain flexibility and its reflection in the conformation statistics. To the best of our knowledge, this dependence has not been discussed in the literature (where shorter chains were predominantly used). Table 2 has shown that for the purpose of property prediction (of course, with the exception of δ), there is not much advantage of increasing N_{DP} beyond 300. Therefore, in all results presented below, each cell (pure PVC or mixture) contains five chains, each of which has $N_{\text{DP}} = 300$. Again, this choice does not affect any of our conclusions. Indeed, as shown later, our prediction of thermodynamic compatibility is not based on the cohesive energy or solubility parameter, but on the heat of mixing, in which the arbitrariness of the reference state is no longer a factor. Nevertheless, we still find

Table 3: Comparison of the density and solubility parameter of pure plasticizers from our MD simulation with experimental values in references

Pure	Density (g/cm ³)		Solubility Parameter ((J/cm ³) ^{1/2})	
	MD (26.85°C)	Expt. (20°C) ⁷⁸	MD (26.85°C)	Ref.(25°C) ^a
DIBP	$1.03 \pm 1.00 \times 10^{-3}$	1.038	$20.0 \pm 4.00 \times 10^{-2}$	18.76
DIOP	$0.950 \pm 3.00 \times 10^{-3}$	0.983	$19.1 \pm 4.00 \times 10^{-2}$	18.10
DINP	$0.937 \pm 1.00 \times 10^{-3}$	0.975	$18.9 \pm 5.00 \times 10^{-2}$	18.04
DIDP	$0.926 \pm 1.00 \times 10^{-3}$	0.967	$18.4 \pm 7.00 \times 10^{-2}$	17.92
DITP	$0.898 \pm 1.00 \times 10^{-3}$	0.952	$18.0 \pm 5.00 \times 10^{-2}$	17.41
DEHP	$0.948 \pm 1.00 \times 10^{-3}$	0.984	$19.2 \pm 1.20 \times 10^{-1}$	18.20
PVC	$1.36 \pm 1.00 \times 10^{-3}$	$1.35 \sim 1.45$ ⁶⁷	$17.1 \pm 2.00 \times 10^{-1}$	19.35 ⁶⁵

^aCalculated by Marcilla and Garcia⁷⁹ using the group contribution method of Small⁸⁰.

it necessary to include this discussion for the importance of cohesive energy calculation in understanding the thermodynamic properties of polymers.

3.1.4 Pure phthalates and PVC-phthalate mixtures

To test the accuracy of our molecular models for pure plasticizers, the density and solubility parameters obtained from our simulation are compared with the experimental references in table 3. Densities calculated from MD are all slightly lower than the experimental values, except DIBP, where the values are much closer. This difference can at least be partially attributed to the slightly lower temperature in the experiments. All computed solubility parameters are higher than the corresponding reference values (which is calculated by a group contribution method⁸⁰), but not by much. For the purpose of this study, comparison between different plasticizers is more important than the absolute values themselves. It is encouraging to note that the simulation results well reflect such comparisons.

In typical industrial applications, around 10 wt% to 40 wt% plasticizers are used. In this study, all mixture cells contain five PVC chains and each has 300 repeating units. The number of plasticizers is adjusted to keep a constant 21wt% between different mixtures.

Table 4: Compositions and densities of the PVC/Plasticizer mixture cells.

	Number of plasticizers	Number of PVC chains	Repeating units per chain	Weight fraction	Final Density (g/cm ³)
DIBP+PVC	90	5	300	0.211	$1.26 \pm 1.00 \times 10^{-3}$
DEHP+PVC	64	5	300	0.210	$1.23 \pm 2.00 \times 10^{-3}$
DIOP+PVC	64	5	300	0.210	$1.24 \pm 1.00 \times 10^{-3}$
DINP+PVC	60	5	300	0.211	$1.23 \pm 2.00 \times 10^{-3}$
DIDP+PVC	56	5	300	0.210	$1.23 \pm 1.00 \times 10^{-3}$
DITP+PVC	47	5	300	0.210	$1.22 \pm 1.00 \times 10^{-3}$

The compositions of all mixture cells are listed in table 4 along with their densities. All plasticized cells have lower density than pure PVC. For most of them, the density is around 1.23 g/cm³. The DIBP case is the only outlier with a higher 1.26 g/cm³. This can be explained considering the chemical structures of the phthalates (table 1) and their interaction with PVC. The CH–Cl groups on PVC are polar and their strong interactions hold chain segments tightly together. Extended non-polar alkyl side chains on phthalates split these groups apart, “un-bond” these interactions, and loosen the packing of PVC. DIBP has much shorter alkyl side chains than the rest and thus less unpacking effect.

3.2 Thermodynamic compatibility

At first, thermodynamic compatibility or miscibility between the components was mainly a consideration for processing: how to adequately blend the constituents into a well-dispersed mixture. Recent concerns caused by plasticizer migration attached new importance to this attribute. Plasticizers with higher affinity with the host polymer have a lower thermodynamic tendency towards migration. The rate of migration is also important. However, for their large molecular size and nontrivial interaction with the host polymer, direct prediction of the diffusion rate from atomistic simulation is not possible for industrial plasticizers. Although penetrant diffusion in polymers is influenced by many factors, for the same polymer matrix,

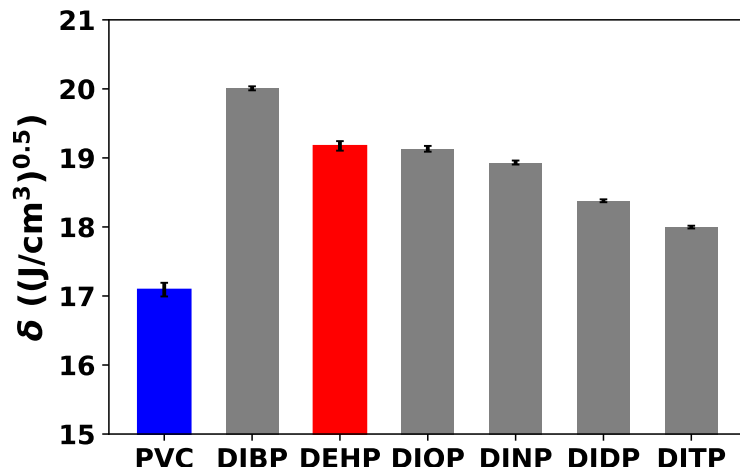


Figure 9: Hildebrand solubility parameters of pure plasticizers compared with that of pure PVC.

the energy barrier for diffusion motion is higher for penetrant molecules that interact more favorably with the host polymer. Therefore, thermodynamic compatibility at least gives a semi-quantitative indication of how the migration tendency of a given plasticizer compares with that of others.

The calculated solubility parameters for the pure plasticizers and PVC (previously listed in table 3) are re-plotted in fig. 9 for easier comparison. Plasticizers all have much higher δ than PVC and its value decreases monotonically with the alkyl side chain length. Note that both DEHP and DIOP have eight-carbon alkyl chains and their solubility parameters are nearly the same. Strong dependence of δ on the alkyl chain length is expected as longer alkyl chains result in a higher proportion of non-polar parts in a molecule, which lowers the cohesive energy. Empirically, the proximity of solubility parameters is often used to estimate the miscibility between components: species with similar δ are expected to mix well. This rule is based on the assumption that the cross-species interaction is approximated by the geometric mean of the self-interactions (in pure species), which is only reasonable for non-polar species with no specific interactions⁸¹. Industrial plasticizers typically interact with their host polymers in a nontrivial manner: for phthalates, their interaction with PVC is a subject of further discussion below. Therefore, predicting plasticizer compatibility with its

host polymer by comparing solubility parameters is no longer appropriate (although misuse is often seen in the literature and other technical documents). For example, as we will show later, DIBP is the most compatible out of all phthalates studied, yet its solubility parameter differs most from that of PVC, and DEHP is more compatible with PVC than DIOP despite their similar δ values. One may recall that our model, same as those of previous MD studies^{17,41,76}, significantly underestimates the δ value for polymers. However, relying on experimentally measured δ for miscibility prediction is itself complicated by its large uncertainty, lack of consistency in measurement techniques (e.g., solvent extraction for PVC and group contribution for plasticizers in tables 2 and 3), and departure from the Hildebrand definition in the polymer case (as discussed above).

Miscibility between components are ultimately determined by the Gibbs energy change of mixing ΔG . Free energy calculation of long-chain polymer systems, especially for temperature close to or below T_g , is computationally prohibitive owing to the enormous time scale for sampling the polymer configuration space. Meanwhile, in practical applications, one is more often only interested in the qualitative estimation of the compatibility. Since industrial plasticizers fall within a reasonable range of size and molecular characteristics, if we assume that polymer conformational changes, when mixed with different plasticizers, are similar, the entropy contribution to ΔG would be small compared with the enthalpy part. Under this premise, the latter, i.e., heat of mixing

$$\Delta H \equiv H_{p+a} - w_p H_p - w_a H_a \tag{7}$$

will be most indicative of the thermodynamic compatibility. Here, H_{p+a} , H_p and H_a are the specific enthalpy of the mixture, pure polymer, and pure additive (plasticizer), respectively, and w_p and w_a are the corresponding mass fractions. The relationship between ΔH and the concepts of cohesive energy and solubility parameter above becomes clear if we neglect the

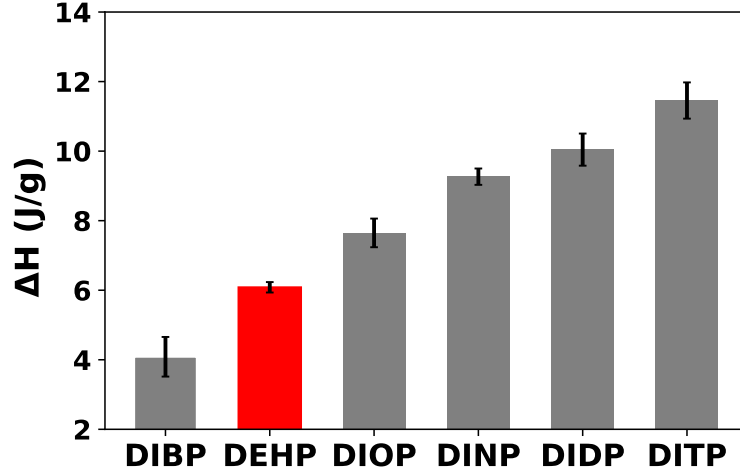


Figure 10: Heat of mixing between PVC and different phthalates.

volume change of mixing ($\Delta V \approx 0$) and substitute (using eqs. (5) and (6))

$$E = E_{\text{sep}} - E_{\text{coh}} = E_{\text{sep}} - \frac{\delta^2}{\rho} \quad (8)$$

into eq. (7) to get

$$\Delta H \approx \Delta E = w_p \frac{\delta_p^2}{\rho_p} + w_a \frac{\delta_a^2}{\rho_a} - E_{\text{coh, p+a}} \quad (9)$$

where

$$E_{\text{coh, p+a}} \equiv w_p E_{\text{sep, p}} + w_a E_{\text{sep, a}} - E_{\text{p+a}} \quad (10)$$

is the specific cohesive energy of the mixture. Note that calculating ΔH from eq. (7) does not require the vacuum reference state E_{sep} any more: the complexity of cohesive energy calculation discussed above is circumvented.

The calculated ΔH for all plasticizer mixtures with PVC is shown in fig. 10. Since higher ΔH indicates lower compatibility, thermodynamic compatibility of these plasticizers with PVC is found to be in the order of : DIBP > DEHP > DIOP \geq DINP > DIDP >

Table 5: Reference values of the Flory-Huggins χ parameter between PVC and selected phthalates⁸².

	χ	
	Expt.	UNIFAC-FV Model
DIBP+PVC	-0.13	–
DEHP+PVC	-0.10	-0.14
DINP+PVC	-0.03	-0.02
DIDP+PVC	-0.01	0.04
DITP+PVC	0.22	0.59

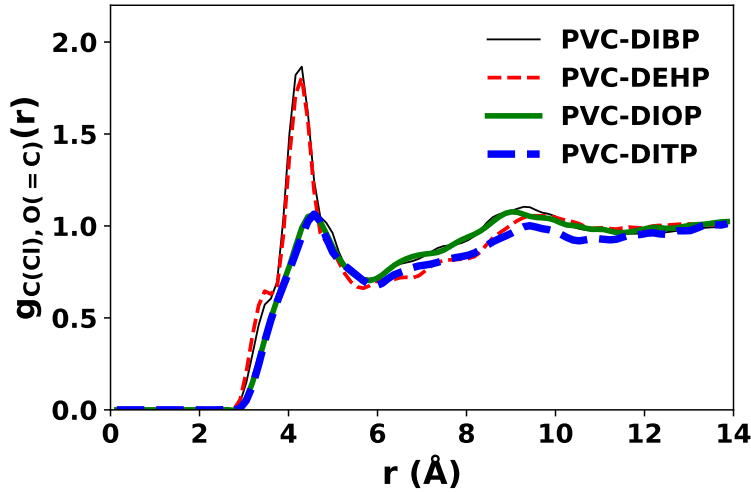


Figure 11: Radial distribution functions (RDFs) between the C atoms bonded with Cl in PVC and the carbonyl O atoms in phthalates $g_{C(Cl),O(=C)}(r)$ in different PVC-phthalate mixtures.

DITP. The result is compared with the Flory-Huggins interaction parameter χ reported by Van Oosterhout and Gilbert⁸² (table 5) in which the experimental χ values were deduced from the solid-gel transition temperature (clear point) in the PVC+plasticizer mixture and the model prediction was based on a group contribution method (UNIFAC-FV). Note that lower χ indicates better compatibility – the order of compatibility from these χ values is fully consistent with our prediction from ΔH . In addition, Erythropel et al.¹⁶ reviewed multiple experimental references and summarized that for diesters their compatibility with PVC peaks at 4 to 6 carbons in the alkyl chains, which again is consistent with our finding.

At the molecular level, it is not hard to understand the higher compatibility of DIBP (4-carbon alkyl chains) compared with DIOP, DINP, DIDP, and DITP (8 to 13-carbon alkyl chains). Inserting plasticizer molecules between PVC chain segments can block the polar-polar interactions between the CH(Cl) groups in PVC. This loss is only partially compensated by the new interactions between CH(Cl) and the carboxyl ester groups in phthalates which are also polar. Many CH(Cl) groups will however be exposed to the non-polar alkyl chains. Blocking of the polymer-polymer interaction is a key mechanism for reducing the inter-segmental friction and for plasticization at least according to the lubricity theory. Meanwhile, the polar part (carboxyl esters) is still necessary for ensuring the miscibility with PVC. The blocking effect obviously becomes more pronounced with increasing alkyl group size, which leads to lower compatibility. What is surprising, however, is that DEHP has the same 8 carbons in the alkyl chains as DIOP but its ΔH is much lower than the latter. The radial distribution function $g_{\text{C(Cl),O(=C)}}(r)$ (fig. 11) measures the average density of carbonyl O atoms (in phthalate carboxyl groups) at a given distance r from C atoms in CH(Cl) of PVC. Comparing DIOP and DITP with DIBP, the first peak (at around 4.33 Å to 4.62 Å becomes much lower because the CH(Cl) group is much more likely to be in contact with the alkyl part than the carboxyl part of the phthalate. However, for DEHP, even though the total number of carboxyl ester groups in the domain is the same as DIOP (compared at the same mass fraction; see table 4), the first peak is nearly as high as that of DIBP (which has more carboxyl ester groups in the cell). Clearly, the different alkyl branching configuration in DEHP, which has a longer (ethyl) branch closer to the carboxyl ester than DIOP (table 1), allows its closer contact and stronger binding with CH(Cl).

3.3 Plasticization effects

We turn now to the comparison of plasticization efficiency of these phthalates. The notion of plasticization effects is not precisely defined and encompasses changes in a broad range of properties. In this study, we focus on two primary aspects of plasticization: reductions of

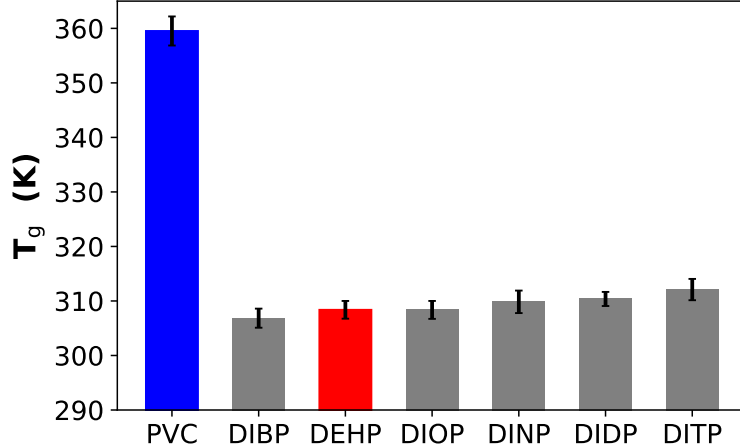


Figure 12: Comparison of T_g of pure PVC and PVC/plasticizer mixtures.

T_g and Young's modulus. Determination of T_g from the temperature dependence of specific volume was discussed above (see section 2.2 and fig. 3) and the results for PVC-plasticizer mixtures are shown in fig. 12. It is clear that at the dosage of 21wt% all phthalates tested have effectively plasticized the PVC materials with a T_g reduction of ≈ 50 K in each case. Variations between plasticizers are comparatively small but there is a clear decline of plasticizer efficiency (higher T_g at the same dosage) with the increasing alkyl chain length. For DEHP and DIOP, which have the same 8-carbon alkyl chains but different branching configurations, the T_g of their mixtures with PVC are nearly the same. This order of plasticization efficiency, i.e., $\text{DIBP} > \text{DIOP} > \text{DINP} > \text{DITP}$, agrees with experimental observations⁷⁸. The result is also consistent with Erythropel et al.¹⁶'s experiments of two other families of diesters (succinates and maleates) that plasticization effects peak at 4 to 6 carbons in the alkyl chains. It however apparently contradicts the classical lubricity theory in which the non-polar parts of the plasticizer molecule – i.e., alkyl chains in phthalates – block the polar-polar interactions between polymer segments and reduce the chain friction. One may note that these phthalates are compared at the same mass fraction – the molar fraction is lower for a plasticizer with higher molecular weight. On the other hand, longer alkyl chains result in a higher percentage of non-polar parts of a plasticizer: e.g., at the same mass fraction, the number of DIBP molecule is around twice that of DITP (see table 4), but the number

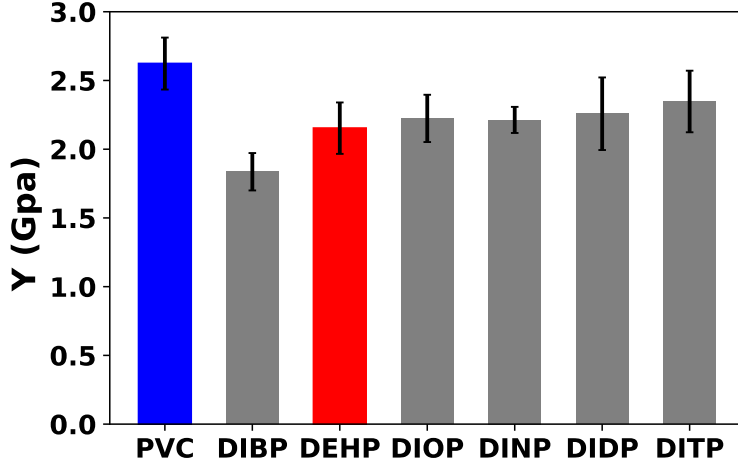


Figure 13: Comparison of the Young's Moduli of pure PVC and PVC/plasticizer mixtures at 300K.

of alkyl carbon atoms per molecule of DITP is more than three times that of DIBP – the total number of alkyl carbon atoms is still higher for DITP. Therefore, at the same level of molar fraction, although not tested here, it is expected that phthalates with longer alkyl chains will be more effective in reducing T_g , which of course will have higher plasticizer mass fraction. Meanwhile, increasing the mass fraction of non-polar groups (alkyl chains) at the same overall mass fraction of plasticizers (as in this study) does not improve T_g reduction for, e.g., DIDP or DITP. The increasing availability of non-polar groups for inter-chain lubrication alone is not sufficient to account for the plasticization effects. At the same mass fraction, smaller plasticizers have more numbers of individual molecules, each of which also has higher mobility. Both can help explain their higher efficiency for plasticization.

Tensile elongation is simulated by stretching the amorphous cell in the z direction with a controlled domain length profile

$$L_z(t) = L_{z,0}(1 + \dot{\epsilon}t) \quad (11)$$

to keep a constant engineering strain rate of $\dot{\epsilon} = 5 \times 10^8 \text{ s}^{-1}$, where $L_{z,0}$ is the equilibrium domain length. A Nosé-Hoover barostat is used to maintain the pressure in x and y directions

at 1 atm. Stress evolution as a function of the engineering strain is recorded every 0.1 ps during the deformation. The relationship between the tensile stress

$$s = -P_z + \frac{1}{2}(P_x + P_y) \quad (12)$$

and engineering strain

$$e \equiv \frac{L_z - L_{z,0}}{L_{z,0}} \quad (13)$$

is initially linear at the limit of small deformation. The slope of the stress-strain curve in that limit is defined as the Young's modulus

$$Y \equiv \lim_{e \rightarrow 0} \frac{ds}{de}. \quad (14)$$

In practice, linear regression is performed on the stress-strain curve for the engineering strain range up to 0.02 to extract the slope. Results for pure PVC and different PVC-plasticizer mixtures are shown in fig. 13 for 300 K which is below the T_g of all cases. Experimental reports of the Young's modulus of pure PVC ranges from 1.0 GPa to 4.0 GPa^{66,83–85}. Our MD result falls well within this range. The agreement is excellent especially considering that the simulation strain rate is higher than that of typical experiments, which rarely goes beyond $O(10^3)\text{s}^{-1}$. The overall trend, i.e., the order of plasticization efficiency of different phthalates, is consistent with that observed in T_g : plasticizers become less effective as the alkyl side chain grow. However, the effect is much more pronounced: the most effective one – DIBP with 4-carbon alkyl chains – reduces the Young's modulus by nearly one third, whereas the Young's modulus of PVC plasticized by DITP (13-carbon) is only slightly reduced compared with pure PVC.

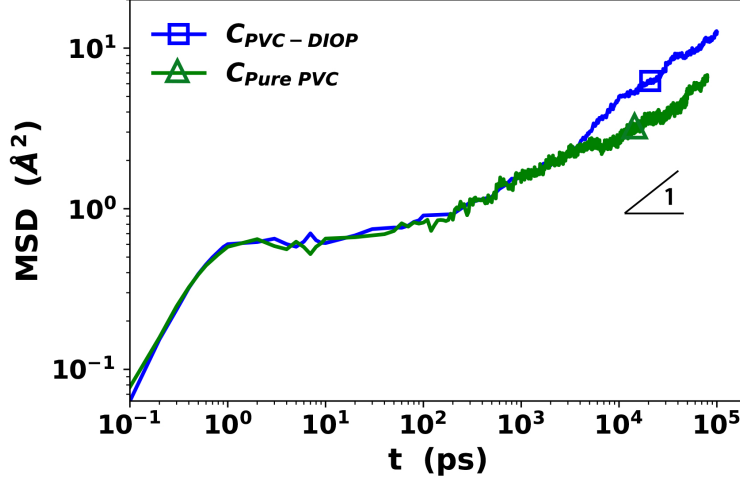


Figure 14: Mean square displacement (MSD) of PVC backbone carbon atoms of pure PVC and PVC/DIOP mixtures at 300K.

3.4 Molecular mobility

We conclude the section by inspecting the microscopic aspect of plasticization – increasing mobility of the constituting atoms and molecules. The mean square displacement (MSD)

$$\langle r^2 \rangle(t) \equiv \langle \vec{r}(t + t_0) - \vec{r}(t_0) \rangle^2 \quad (15)$$

(\vec{r} is the atom position, t_0 is the reference time origin, and $\langle \cdot \rangle$ denotes average over all t_0 and all atoms) of carbon atoms on the polymer backbones is plotted in fig. 14 for pure PVC and that plasticized by DIOP. Both curves start with a super-diffusive regime in the short-time limit, where the slope of $\log \langle r \rangle$ vs. $\log t$ exceeds 1. After $t \sim O(1)$ ps, a clear plateau is found where $\langle r^2 \rangle$ increases very little over more than two decades of time scales. This is typical of glassy liquids where atoms are dynamically arrested by their neighboring atoms, the so-called “caging” effect, and only localized segmental motion (the “ β -process”) is possible^{86,87}. (Note that occurrence of this plateau stage is not unique for polymers – it is also observed in small-molecule supercooled liquids⁸⁸.) Between $O(100)$ ps $\leq t \leq O(1000)$ ps, the curves start to lift up again, as the cooperative motion of atoms or segments starts to allow larger scale molecular relaxation (transition to the “ α -process”). The slope is initially smaller than

1, indicative of sub-diffusive dynamics. The plasticized case eventually reaches the Fickian diffusion regime where $\langle r^2 \rangle \propto t$ at $t \gtrsim 5000\text{ps}$, whereas for the pure PVC case this occurs at some time scale beyond reach by our simulation.

Previous studies of pure polymers^{87,88} have shown that the plateau emerges as T approaches T_g from the upper side. With falling T , the plateau increases in length and decreases in height – less MSD is observed within this dynamically arrested regime. This trend continues as T drops below T_g ⁸⁸. Interestingly, the MSD curves of pure and plasticized PVC almost completely overlap within both the plateau and the sub-diffusive regime: i.e., adding DIOP does not seem to affect the PVC chain motions in these time scales. Separation only occurs at much longer time scale as the plasticized PVC first enters the diffusive regime. Note that $T = 300\text{ K}$ (used in fig. 14) is only a few degrees lower than the T_g of the PVC-DIOP mixture and over 50 degrees lower than that of pure PVC (fig. 12). This suggests that the dynamics of pure and plasticized polymers are not comparable at the same non-dimensional temperature T/T_g . Meanwhile, at the same T , the relaxation behaviors of the two cases are nearly the same in the dynamically arrested state, suggesting that a simple free-volume argument, that small-molecule additives create more space between chain segments, is not sufficient for explaining plasticization. Instead, adding plasticizers seems to induce an earlier onset of the cooperative motion and α -relaxation process. This observation poses new questions for understanding the glass transition dynamics of plasticized polymer mixtures.

MSD is also calculated for different parts of the phthalate molecules in fig. 15. We track the carbon atoms on the aromatic ring for the motion of the head of the molecule and those on the alkyl chains for the legs. MSD of the backbone of PVC in the same mixture is plotted for comparison. For both DIBP and DITP, all three curves show similar trends: they all start with a super-diffusive range, a plateau of dynamical arrest, a short sub-diffusive range, and eventually the diffusive range at the long time limit. Not surprisingly, the PVC curve lies below those of the plasticizer, which reflects the topological constraints from the chain length and the resulting longer relaxation time. Comparing different parts of the phthalate

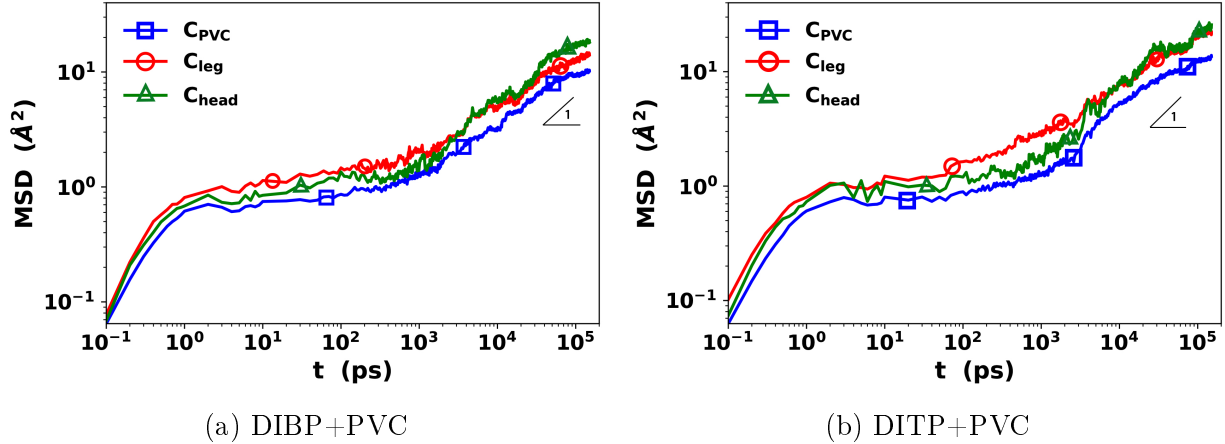


Figure 15: Mean square displacement of carbon atoms in the head (aromatic ring) and legs (alkyl chains) of DIBP and DITP compared with that of the PVC backbone in the same mixture (300 K).

molecules, the aromatic ring (head) shows lower mobility than the alkyl chains (legs) in the super-diffusive, plateau, and sub-diffusive regimes, which again is expected owing to its bulky structure and the stronger polar-polar interactions of their adjacent ester groups with PVC. Interestingly, MSD of the head surpasses that of the legs as it rises to the diffusive regime ($\langle r^2 \rangle \propto t$) earlier: i.e., the long-time relaxation or diffusion of phthalates is driven by the movement of the heads, with the legs still trapped between polymer segments and other plasticizer molecules. Because of the computational cost of obtaining these MSD curves (from MD of 150ns), we are not able to repeat these simulations with independent configurations for error bars. However, observing the same trend in two different phthalate cases indicates that it is unlikely a result of statistical noise. This observation can be explained considering that relaxation of long alkyl chains is not much different from that of polymers: owing to its flexibility, the alkyl chain must explore a large number of configurational possibilities before it is able to navigate the confinement by the surrounding polymers. Diffusion rate is the other important factor (the first one is thermodynamic compatibility examined above) that determines the migration-resistance of plasticizers. The finding here suggests that the constrained relaxation of non-polar side chains has important influence on the migration rate. It may also explain why DEHP, despite its better thermodynamic compatibility with

PVC (fig. 10), is more prone to migration loss under heat than DINP and DIDP in industrial tests⁸⁹. The alkyl side chains in DEHP is more branched than those in DIOP (both cases have 8 carbon atoms in each side chain) and it is known that for the same molecular weight, branched polymers have lower friction and thus faster relaxation than linear chains⁹⁰. Integrating theories of polymer dynamics into the prediction of plasticizer migration is one of our future focuses. On the other hand, however, it is unclear how slowing down the plasticizer relaxation (for better migration resistance) might affect its plasticization efficacy. Much future research is needed.

4 Conclusions

We report the first systematic investigation of the performance of common phthalates as plasticizers for PVC. A multi-step simulation protocol for preparing and equilibrating full-atom molecular models for amorphous polymer-plasticizer mixtures are thoroughly tested for statistically robust materials property prediction. Thermodynamic compatibility of phthalate molecules with PVC and their plasticization efficacy are predicted and the results are in agreement with all known experimental observations. For phthalates with the same alkyl side chain configuration, increasing the length of these chains results in worse compatibility with PVC and worse plasticization outcome. Especially, Young’s modulus reduction diminishes quickly with plasticizer size and for the largest one tested (DITP), the Young’s modulus of the mixture is fairly close to pure PVC. Comparing DEHP and DIOP, two phthalates with the same number of carbons in the alkyl chain but different branching configurations, DEHP is significantly more compatible with PVC but their plasticization efficiencies are similar. For DEHP, having a longer (ethyl) branch closer to the ester group in the alkyl chain makes it easier to maintain stronger polar-polar interaction with PVC.

Molecular mobility of different components is investigated with their MSD in the glassy state for an extended period of time. Despite an over 50 K drop in T_g , relaxation dynamics

of the carbon backbone of plasticized PVC in its glassy state is nearly identical to that of pure PVC for the entire short-time regime (dynamically-arrested and sub-diffusive regimes). Plasticization is only reflected in the long-time relaxation where the plasticized polymer chains escape the dynamically-arrested stage at shorter time scales. Mobility of the plasticizers show that although the aromatic ring shows slower short-time dynamics, it escapes the caging constraint earlier than the alkyl side chains. Design of the side chain configuration is important for improving their migration resistance.

Implication of the study is twofold. First, by testing the prediction reliability of our molecular models for the most commonly used industrial plasticizers, we have established a simulation protocol that can be used to examine newer alternative plasticizers for comprehensive performance evaluation. Second, molecular insight stemming from the comparison between these phthalates is an important guideline for the molecular design. On the other hand, we also recognize two important considerations in the calculation of cohesive energy and solubility parameter of polymers. The first is the ambiguity of the vacuum reference state, which was first studied by Choi⁵² but still often overlooked. The second is the non-trivial chain-length dependence for long-chain polymers, which we report for the first time. A mechanism for the latter is proposed in this paper.

Acknowledgment

The authors acknowledge the financial support by the Natural Sciences and Engineering Research Council (NSERC) of Canada (RGPIN-4903-2014, EGP-492469-2015, CRDPJ-514051-17) and Canadian General Tower, Ltd. We also acknowledge Compute/Calcul Canada for its allocation of computing resource. DL would like to thank the China Scholarship Council (CSC) for supporting his doctoral study at McMaster University (No. 201500090106). This work is also made possible by the facilities of the Shared Hierarchical Academic Research Computing Network (SHARCNET: www.sharcnet.ca).

References

- (1) Tizazu Mekonnen, Paolo Mussone, Hamdy Khalil, and David Bressler. Progress in bio-based plastics and plasticizing modifications. *Journal of Materials Chemistry A*, 1 (43):13379–13398, 2013.
- (2) Malcolm P Stevens. *Polymer Chemistry: An Introduction*. Oxford University Press, New York, 1999.
- (3) John Murphy. *Additives for plastics handbook*. Elsevier, 2001.
- (4) Joel A Tickner, Ted Schettler, Tee Guidotti, Michael McCally, and Mark Rossi. Health risks posed by use of di-2-ethylhexyl phthalate (dehp) in pvc medical devices: A critical review. *American journal of industrial medicine*, 39(1):100–111, 2001.
- (5) Federica Chiellini, Marcella Ferri, Andrea Morelli, Lucia Dipaola, and Giuseppe Latini. Perspectives on alternatives to phthalate plasticized poly (vinyl chloride) in medical devices applications. *Progress in Polymer Science*, 38(7):1067–1088, 2013.
- (6) Giuseppe Latini. Monitoring phthalate exposure in humans. *Clinica Chimica Acta*, 361 (1-2):20–29, 2005.
- (7) M. Hakkarainen. Migration of monomeric and polymeric PVC plasticizers. In A. - C. Albertsson and M. Hakkarainen, editors, *Chromatography for sustainable polymeric materials*, volume 211 of *Advances in Polymer Science*, pages 159–185. Springer, Berlin, 2008. doi: 10.1007/12_2008_140.
- (8) Mustafizur Rahman and Christopher S Brazel. The plasticizer market: an assessment of traditional plasticizers and research trends to meet new challenges. *Progress in polymer science*, 29(12):1223–1248, 2004.
- (9) L. Bernard, B. Décaudin, M. Lecoœur, D. Richard, D. Bourdeaux, R. Cueff, V. Sautou, and ARMED Study Group. Analytical methods for the determination of DEHP plasti-

- cizer alternatives present in medical devices: A review. *Talanta*, 129:39–54, 2014. doi: 10.1016/j.talanta.2014.04.069.
- (10) Ezekiel H Hull. Citrate esters and methods, April 25 1989. US Patent 4,824,893.
 - (11) Brian L Wadey. An innovative plasticizer for sensitive applications. *Journal of Vinyl and Additive Technology*, 9(4):172–176, 2003.
 - (12) Yuki Ito, Toshiki Nakamura, Yukie Yanagiba, Doni Hikmat Ramdhan, Nozomi Yamagishi, Hisao Naito, Michihiro Kamijima, Frank J Gonzalez, and Tamie Nakajima. Plasticizers may activate human hepatic peroxisome proliferator-activated receptor α less than that of a mouse but may activate constitutive androstane receptor in liver. *PPAR research*, 2012, 2012.
 - (13) Mustafizur Rahman and Christopher S Brazel. Ionic liquids: New generation stable plasticizers for poly (vinyl chloride). *Polymer Degradation and Stability*, 91(12):3371–3382, 2006.
 - (14) Paul H Daniels. A brief overview of theories of pvc plasticization and methods used to evaluate pvc-plasticizer interaction. *Journal of vinyl and additive technology*, 15(4): 219–223, 2009.
 - (15) George Wypych. *Handbook of plasticizers*. ChemTec Publishing, 2004.
 - (16) Hanno C Erythropel, Sarah Shipley, Aurélie Börmann, Jim A Nicell, Milan Maric, and Richard L Leask. Designing green plasticizers: Influence of molecule geometry and alkyl chain length on the plasticizing effectiveness of diester plasticizers in pvc blends. *Polymer*, 89:18–27, 2016.
 - (17) D. N. Theodorou and U. W. Suter. Detailed molecular-structure of a vinyl polymer glass. *Macromolecules*, 18:1467–1478, 1985. doi: 10.1021/ma00149a018.

- (18) D. Curc3, D. Zanuy, and C. Alem3n. EVEBAT: A fast strategy for the examination of the empty space in polymer matrices. *J. Comput. Chem.*, 24:1208–1214, 2003.
- (19) P. Carbone, H. A. Karimi-Varzaneh, and F. M3ller-Plathe. Fine-graining without coarse-graining: an easy and fast way to equilibrate dense polymer melts. *Faraday Discuss.*, 144:25–42, 2010. doi: {10.1039/b902363a}.
- (20) L. J. Abbott, K. E. Hart, and C. M. Colina. Polymatic: a generalized simulated polymerization algorithm for amorphous polymers. *Theor. Chem. Acc.*, 132:1334, 2013. doi: {10.1007/s00214-013-1334-z}.
- (21) Peter J. Ludovice and Ulrich W. Suter. Detailed molecular structure of a polar vinyl polymer glass. In Jozef Bicerano, editor, *Computational Modeling of Polymers*, chapter 8, pages 401–438. CRC Press, New York, 1992. ISBN 978-0824784386.
- (22) Vlasios G. Mavrantzas, Travis D. Boone, Evangelia Zervopoulou, and Doros N. Theodorou. End-bridging Monte Carlo: a fast algorithm for atomistic simulation of condensed phases of long polymer chains. *Macromolecules*, 32:5072–5096, 1999. doi: 10.1021/ma981745g.
- (23) Nikos Ch Karayiannis, Vlasios G Mavrantzas, and Doros N Theodorou. A novel monte carlo scheme for the rapid equilibration of atomistic model polymer systems of precisely defined molecular architecture. *Physical review letters*, 88(10):105503, 2002.
- (24) VA Harmandaris, NP Adhikari, Nico FA van der Vegt, and Kurt Kremer. Hierarchical modeling of polystyrene: From atomistic to coarse-grained simulations. *Macromolecules*, 39(19):6708–6719, 2006.
- (25) Christine Peter and Kurt Kremer. Multiscale simulation of soft matter systems—from the atomistic to the coarse-grained level and back. *Soft Matter*, 5(22):4357–4366, 2009.

- (26) R. M. Sok, H. J. C. Berendsen, and W. F. van Gunsteren. Molecular-dynamics simulation of the transport of small molecules across a polymer membrane. *J. Chem. Phys.*, 96:4699–4704, 1992.
- (27) M. L. Greenfield and D. N. Theodorou. Molecular modeling of methane diffusion in glassy atactic polypropylene via multidimensional transition state theory. *Macromolecules*, 31:7068–7090, 1998. doi: 10.1021/ma980750h.
- (28) M. L. Greenfield and D. N. Theodorou. Coarse-grained molecular simulation of penetrant diffusion in a glassy polymer using reverse, and kinetic Monte Carlo. *Macromolecules*, 34:8541–8553, 2001. doi: 10.1021/ma002157h.
- (29) S Neyertz, D Brown, Sudharsan Pandiyan, and Nico FA van der Vegt. Carbon dioxide diffusion and plasticization in fluorinated polyimides. *Macromolecules*, 43(18):7813–7827, 2010.
- (30) Liling Zhang, Youchang Xiao, Tai-Shung Chung, and Jianwen Jiang. Mechanistic understanding of co₂-induced plasticization of a polyimide membrane: A combination of experiment and simulation study. *Polymer*, 51(19):4439–4447, 2010.
- (31) L. Xi, M. Shah, and B. L. Trout. Hopping of water in a glassy polymer studied via transition path sampling and likelihood maximization. *J. Phys. Chem. B*, 117:3634–3647, 2013. doi: 10.1021/jp3099973.
- (32) Hakima Abou-Rachid, Louis-Simon Lussier, Sophie Ringuette, Xavier Lafleur-Lambert, Mounir Jaidann, and Josée Brisson. On the correlation between miscibility and solubility properties of energetic plasticizers/polymer blends: modeling and simulation studies. *Propellants, Explosives, Pyrotechnics*, 33(4):301–310, 2008.
- (33) Jasmine Gupta, Cletus Nunes, Shyam Vyas, and Sriramakamal Jonnalagadda. Prediction of solubility parameters and miscibility of pharmaceutical compounds by molecular dynamics simulations. *The Journal of Physical Chemistry B*, 115(9):2014–2023, 2011.

- (34) Yu Zhao, Xiaohong Zhang, Wei Zhang, Hongjun Xu, Wuxi Xie, Jiaojiao Du, and Yingzhe Liu. Simulation and experimental on the solvation interaction between the gap matrix and insensitive energetic plasticizers in solid propellants. *The Journal of Physical Chemistry A*, 120(5):765–770, 2016.
- (35) Karl G Wagner, Martin Maus, Andreas Kornherr, and Gerhard Zifferer. Glass transition temperature of a cationic polymethacrylate dependent on the plasticizer content—simulation vs. experiment. *Chemical physics letters*, 406(1-3):90–94, 2005.
- (36) Junqing Yang, Xueli Zhang, Pin Gao, Xuedong Gong, and Guixiang Wang. Molecular dynamics and dissipative particle dynamics simulations of the miscibility and mechanical properties of GAP/DIANP blending systems. *RSC Adv.*, 4:41934–41941, 2014. doi: 10.1039/C4RA04236K.
- (37) Doros N. Theodorou and Ulrich W. Suter. Atomistic modeling of mechanical properties of polymeric glasses. *Macromolecules*, 19:139–154, 1986. doi: 10.1021/ma00155a022.
- (38) Hisao Takeuchi and Ryong-Joon Roe. Molecular dynamics simulation of local chain motion in bulk amorphous polymers. ii. dynamics at glass transition. *The Journal of chemical physics*, 94(11):7458–7465, 1991.
- (39) P. -H. Lin and R. Khare. Molecular simulation of cross-linked epoxy and epoxy-POSS nanocomposite. *Macromolecules*, 42:4319–4327, 2009. doi: {10.1021/ma9004007}.
- (40) D Hossain, MA Tschopp, DK Ward, JL Bouvard, P Wang, and MF Horstemeyer. Molecular dynamics simulations of deformation mechanisms of amorphous polyethylene. *Polymer*, 51(25):6071–6083, 2010.
- (41) Zhonglin Luo and Jianwen Jiang. Molecular dynamics and dissipative particle dynamics simulations for the miscibility of poly (ethylene oxide)/poly (vinyl chloride) blends. *Polymer*, 51(1):291–299, 2010.

- (42) Jean-Louis Barrat, Jörg Baschnagel, and Alexey Lyulin. Molecular dynamics simulations of glassy polymers. *Soft Matter*, 6(15):3430–3446, 2010.
- (43) J. Liu, L. Zhang, D. Cao, J. Shen, and Y. Gao. Computational simulation of elastomer nanocomposites: current progress and future challenges. *Rubber Chem. Technol.*, 85: 450–481, 2012. doi: {10.5254/rct.12.87966}.
- (44) Emmanuel N. Skountzos, Alexandros Anastassiou, Vlas G. Mavrantzas, and Doros N. Theodorou. Determination of the Mechanical Properties of a Poly (methyl methacrylate) Nanocomposite with Functionalized Graphene Sheets through Detailed Atomistic Simulations. *Macromolecules*, 47:8072–8088, 2014. doi: 10.1021/ma5017693.
- (45) Fardin Khabaz and Rajesh Khare. Glass transition and molecular mobility in styrene-butadiene rubber modified asphalt. *J. Phys. Chem. B*, 119:14261–14269, 2015. doi: {10.1021/acs.jpcc.5b06191}.
- (46) Shimiao Zhang and Li Xi. Effects of precursor topology on polymer networks simulated with molecular dynamics. *Polymer*, 116:143–152, 2017. doi: 10.1016/j.polymer.2017.03.048.
- (47) Florian Müller-Plathe. Diffusion of penetrants in amorphous polymers: A molecular dynamics study. *The Journal of chemical physics*, 94(4):3192–3199, 1991.
- (48) Dieter Hofmann, Lydia Fritz, Jens Ulbrich, Claudia Schepers, and Martin Böhning. Detailed-atomistic molecular modeling of small molecule diffusion and solution processes in polymeric membrane materials. *Macromolecular theory and simulations*, 9(6): 293–327, 2000.
- (49) Farkhondeh Mozaffari, Hossein Eslami, and Jalil Moghadasi. Molecular dynamics simulation of diffusion and permeation of gases in polystyrene. *Polymer*, 51(1):300–307, 2010.

- (50) M Belmares, M Blanco, WA Goddard, RB Ross, G Caldwell, S-H Chou, J Pham, PM Olofson, and Cristina Thomas. Hildebrand and hansen solubility parameters from molecular dynamics with applications to electronic nose polymer sensors. *Journal of computational chemistry*, 25(15):1814–1826, 2004.
- (51) Ahmed Jarray, Vincent Gerbaud, and Mehrdji Hemati. Polymer-plasticizer compatibility during coating formulation: A multi-scale investigation. *Progress in Organic Coatings*, 101:195–206, 2016.
- (52) Phillip Choi. A Re-Examination of the Concept of Hildebrand Solubility Parameter for Polymers. *Macromol. Rapid Commun*, 23:484–487, 2002. doi: 10.1002/1521-3927(20020501)23:8<484::AID-MARC484>3.0.CO;2-K.
- (53) J. R. Maple, M. J. Hwang, T. P. Stockfisch, U. Dinur, M. Waldman, C. S. Ewig, and A. T. Hagler. Derivation of class-II force-fields .1. Methodology and quantum force-field for the alkyl functional-group and alkane molecules. *J. Comput. Chem.*, 15:162–182, 1994.
- (54) MJ Hwang, TP Stockfisch, and AT Hagler. Derivation of class ii force fields. 2. derivation and characterization of a class ii force field, cff93, for the alkyl functional group and alkane molecules. *Journal of the American Chemical Society*, 116(6):2515–2525, 1994.
- (55) Abolfazl Noorjahan and Phillip Choi. Thermodynamic properties of poly(vinyl alcohol) with different tacticities estimated from molecular dynamics simulation. *Polymer*, 54: 4212–4219, 2013. doi: 10.1016/J.POLYMER.2013.05.073.
- (56) Steve Plimpton, Paul Crozier, and Aidan Thompson. Lammmps-large-scale atomic/-molecular massively parallel simulator. *Sandia National Laboratories*, 18:43–43, 2007.
- (57) Huai Sun. Compass: an ab initio force-field optimized for condensed-phase applications

- overview with details on alkane and benzene compounds. *The Journal of Physical Chemistry B*, 102(38):7338–7364, 1998.
- (58) M. P. Allen and D. J. Tildesley. *Computer Simulation of Liquids*. Oxford University Press, New York, 1989.
- (59) D. Frenkel and B. Smit. *Understanding Molecular Simulation: from Algorithms to Applications*. Academic Press, London, 2nd edition, 2002.
- (60) P. P. Ewald. The calculation of optical and electrostatic grid potential. *Annalen Der Physik*, 64:253–287, 1921.
- (61) W. Shinoda, M. Shiga, and M. Mikami. Rapid estimation of elastic constants by molecular dynamics simulation under constant stress. *Phys. Rev. B*, 69:134103, 2004. doi: 10.1103/PhysRevB.69.134103.
- (62) Sergei Shenogin and Rahmi Ozisik. Xenoview. <http://xenoview.mat.rpi.edu>, 2010.
- (63) Panagiotis Barmapalexis, Anna Karagianni, and Kyriakos Kachrimanis. Molecular simulations for amorphous drug formulation: Polymeric matrix properties relevant to hot-melt extrusion. *Eur. J. Pharm. Sci.*, 119:259–267, 2018. doi: 10.1016/J.EJPS.2018.04.035.
- (64) Leandro Martínez, Ricardo Andrade, Ernesto G Birgin, and José Mario Martínez. Packmol: a package for building initial configurations for molecular dynamics simulations. *Journal of computational chemistry*, 30(13):2157–2164, 2009.
- (65) Allan F. M. Barton. Solubility parameters. *Chem. Rev.*, 75:731–753, 1975. doi: 10.1021/cr60298a003.
- (66) Charles E Wilkes, JW Summers, CA Daniels, and MT Berard. Pvc handbook 2005. *Hanser, München*, pages 379–384, 2005.

- (67) MV Titow. *PVC technology*. Springer Science & Business Media, 2012.
- (68) Javier Sacristan and Carmen Mijangos. Free volume analysis and transport mechanisms of pvc modified with fluorothiophenol compounds. a molecular simulation study. *Macromolecules*, 43(17):7357–7367, 2010.
- (69) Basel F Abu-Sharkh. Glass transition temperature of poly (vinylchloride) from molecular dynamics simulation: explicit atom model versus rigid ch2 and chcl groups model. *Computational and Theoretical Polymer Science*, 11(1):29–34, 2001.
- (70) Lewis J Fetters, David J. Lohse, Scott T. Milner, and William W. Graessley. *Macromolecules*, 32:6847–6851. doi: 10.1021/MA990620O.
- (71) Armand Soldera and Nouredine Metatla. Glass transition of polymers: Atomistic simulation versus experiments. *Physical Review E*, 74(6):061803, 2006.
- (72) Timothy W Sirk, Ketan S Khare, Mir Karim, Joseph L Lenhart, Jan W Andzelm, Gregory B McKenna, and Rajesh Khare. High strain rate mechanical properties of a cross-linked epoxy across the glass transition. *Polymer*, 54(26):7048–7057, 2013.
- (73) Dirk Willem van Krevelen and Klaas te Nijenhuis. *Properties of polymers: their correlation with chemical structure; their numerical estimation and prediction from additive group contributions*. Elsevier, Amsterdam and Oxford, 4th edition, 2009.
- (74) C A Angell. The old problems of glass and the glass transition, and the many new twists. *Proc. Natl. Acad. Sci. U. S. A.*, 92:6675–6682, 1995. doi: 10.1073/PNAS.92.15.6675.
- (75) Christopher M. Evans, Hui Deng, Wolter F. Jager, and John M. Torkelson. Fragility is a Key Parameter in Determining the Magnitude of T_g-Confinement Effects in Polymer Films. *Macromolecules*, 46:6091–6103, 2013. doi: 10.1021/ma401017n.
- (76) Liang Wu, Long Chen, and Huai Sun. On accuracy of predicting densities and solubility

- parameters of polymers using atomistic simulations. *Mol. Simul.*, 43:510–518, 2017. doi: 10.1080/08927022.2016.1269258.
- (77) Liyan Zhao and Phillip Choi. Study of the correctness of the solubility parameters obtained from indirect methods by molecular dynamics simulation. *Polymer*, 45:1349–1356, 2004. doi: 10.1016/J.POLYMER.2003.03.003.
- (78) David F Cadogan and Christopher J Howick. Plasticizers. *Kirk-Othmer Encyclopedia of Chemical Technology*, 1996.
- (79) A Marcilla and JC Garcia. Rheological study of pvc plastisols during gelation and fusion. *European polymer journal*, 33(3):349–355, 1997.
- (80) P. A. Small. Some factors affecting the solubility of polymers. *J. Appl. Chem*, 3:71–80, 1953. doi: 10.1002/jctb.5010030205.
- (81) M. Rubinstein and R. H. Colby. *Polymer Physics*. Oxford University Press, New York, 2003.
- (82) JT Van Oosterhout and M Gilbert. Interactions between pvc and binary or ternary blends of plasticizers. part i. pvc/plasticizer compatibility. *Polymer*, 44(26):8081–8094, 2003.
- (83) George Wypych. *PVC formulary*. ChemTec Pub., 2009.
- (84) Karl-Heinrich Grote and Erik K Antonsson. *Springer handbook of mechanical engineering*, volume 10. Springer Science & Business Media, 2009.
- (85) R Hernandez, JJ Pena, L Irusta, and A Santamaria. The effect of a miscible and an immiscible polymeric modifier on the mechanical and rheological properties of pvc. *European Polymer Journal*, 36(5):1011–1025, 2000.

- (86) Grant D. Smith and Dmitry Bedrov. Relationship between the α - and β -relaxation processes in amorphous polymers: Insight from atomistic molecular dynamics simulations of 1,4-polybutadiene melts and blends. *J. Polym. Sci. Pt. B-Polym. Phys.*, 45: 627–643, 2007. doi: 10.1002/polb.21064.
- (87) W. Paul, D. Bedrov, and G. D. Smith. Glass transition in 1,4-polybutadiene: Mode-coupling theory analysis of molecular dynamics simulations using a chemically realistic model. *Phys. Rev. E*, 74:021501, 2006. doi: 10.1103/PhysRevE.74.021501.
- (88) D. Fragiadakis and C. M. Roland. Role of structure in the α and β dynamics of a simple glass-forming liquid. *Phys. Rev. E*, 95:022607, 2017. doi: 10.1103/PhysRevE.95.022607.
- (89) Michael Schiller. *PVC Additives: Performance, Chemistry, Developments, and Sustainability*. Hanser Publications, Cincinnati, 2015.
- (90) Jaroslaw T. Bosko, B. D. Todd, and Richard J. Sadus. Viscoelastic properties of dendrimers in the melt from nonequilibrium molecular dynamics. *J. Chem. Phys.*, 121: 12050–12059, 2004. doi: 10.1063/1.1818678.

for Table of Contents use only

Title: An atomistic evaluation of the compatibility and plasticization efficacy of phthalates in poly(vinyl chloride)

Author: Dongyang Li, Kushal Panchal, Roozbeh Mafi, Li Xi

